

Increased and ectopic expression of *Triticum polonicum* VRT-A2 underlies elongated glumes and grains in hexaploid wheat in a dosage-dependent manner

Nikolai M. Adamski¹, James Simmonds¹, Jemima F. Brinton^{1,3}, Anna E. Backhaus¹, Yi Chen¹, Mark Smedley¹, Sadiye Hayta¹, Tobin Florio¹, Pamela Crane¹, Peter Scott^{1,4}, Alice Pieri¹, Olyvia Hall^{1,5}, J. Elaine Barclay¹, Myles Clayton², John H. Doonan², Candida Nibau², Cristobal Uauy¹

¹ John Innes Centre, Norwich Research Park, Norwich NR4 7UH, United Kingdom

² The National Plant Phenomics Centre, Institute of Biological, Rural and Environmental Sciences (IBERS), Aberystwyth University, Gogerddan, Aberystwyth, SY23 3EE UK

Present address:

³ Department of Natural Capital and Plant Health, Royal Botanic Gardens, Kew, Richmond, UK

⁴ Department of Crops & Soils, Scotland's Rural College, Peter Wilson Building, King's Buildings, W Mains Rd, Edinburgh, EH9 3JG

⁵ School of Biological Sciences, University of Reading, Reading RG6 6AH, United Kingdom

Corresponding author: cristobal.uauy@jic.ac.uk

Short title: VRT-A2 encodes the wheat long glume *PI* locus

Keywords: wheat, expression, ectopic, SVP, MADS-box, dosage-dependent, glume, lemma, grain, intron 1

Email address:

Nikolai M. Adamski	nikolai.adamski@jic.ac.uk
James Simmonds	james.simmonds@jic.ac.uk
Jemima F. Brinton	j.brinton@kew.org
Anna E. Backhaus	anna.backhaus@jic.ac.uk
Yi Chen	andy.chen@jic.ac.uk
Mark Smedley	mark.smedley@jic.ac.uk
Sadiye Hayta	sadiye.hayta@jic.ac.uk
Tobin Florio	tobin.florio@jic.ac.uk
Pamela Crane	pamela.crane@jic.ac.uk
Peter Scott	peter.scott@sruc.ac.uk
Alice Pieri	alice.pieri@santannapisa.it
Olyvia Hall	olyviahall@hotmail.co.uk
Elaine Barclay	elaine.barclay@jic.ac.uk
Myles Clayton	mjc18@aber.ac.uk
John Doonan	jhd2@aber.ac.uk
Candida Nibau	csn@aber.ac.uk
Cristobal Uauy	cristobal.uauy@jic.ac.uk

Abstract

Flower development is a major determinant of yield in crops. In wheat, natural variation for the size of spikelet and floral organs is particularly evident in *Triticum polonicum*, a tetraploid subspecies of wheat with long glumes, lemmas, and grains. Using map-based cloning, we identified *VRT2*, a MADS-box transcription factor belonging to the *SVP* family, as the gene underlying the *P1* locus. The causal *P1* mutation is a sequence substitution in intron-1 that results in both increased and ectopic expression of the *T. polonicum VRT-A2* allele. Based on allelic variation studies, we propose that the intron-1 mutation in *VRT-A2* is the unique *T. polonicum* species defining polymorphism, which was later introduced into hexaploid wheat via natural hybridizations. Near-isogenic lines differing for the *T. polonicum* long-glume (*P1*) locus revealed a gradient effect of *P1* across florets. Transgenic lines of hexaploid wheat carrying the *T. polonicum VRT-A2* allele show that expression levels of *VRT-A2* are highly correlated with spike, glume, grain, and floral organ length. These results highlight how changes in expression profiles, through variation in *cis*-regulation, can impact on agronomic traits in a dosage-dependent manner in polyploid crops.

Introduction

The genus *Triticum* contains multiple wheat subspecies exhibiting traits of agronomic interest, making them valuable genetic resources for breeding. Among these, *Triticum turgidum* ssp. *polonicum* (Polish wheat), a tetraploid (AABB) spring wheat, is characterized by elongated glumes and grains, the latter of which is an important component of crop yield. Glumes are sterile bract-like organs that subtend the spikelet. In wheat, each spikelet consists of several florets, which in turn consist of two leaf-like sheathing structures, the lemma and the palea, as well as two lodicules, three stamens and a pistil (Figure 1A).

It was established over 100 years ago that glume length in *T. polonicum* is controlled by a single locus (Biffen, 1905; Engledow, 1920). The *P* or *PI* locus (from Polish wheat) was mapped to chromosome 7A (Matsumura, 1950) and subsequent studies refined the map location to the short arm of chromosome 7A (Watanabe *et al.*, 1996; Kosuge *et al.*, 2010; Okamoto and Takumi, 2013). While *T. polonicum* as a subspecies is defined by its highly elongated glumes, Biffen (1905), Engledow (1920), and Okamoto and Takumi (2013) also observed that the long-glume trait was completely linked with elongated grains, suggesting multiple pleiotropic effects of the *PI* locus. Okamoto and Takumi (2013) further showed that the *T. polonicum* *PI* allele was also linked to an increase in spike length and a reduction in the number of spikelets per spike. These studies all determined a semi-dominant effect of *PI*, with heterozygous lines being intermediate to the parents for both glume and grain length.

In addition to tetraploid *T. polonicum*, there are a number of hexaploid bread wheat accessions with elongated glumes. These include the Chinese landrace *T. petropavlovskyi* (also called ‘Daosuimai’ or rice-head wheat) as well as members of the Portuguese landrace group ‘Arrancada’. It is hypothesized that the long-glume phenotype of these hexaploid wheat accessions is the result of natural hybridisation between *T. polonicum* and local landraces (Chen *et al.*, 1985; Chen *et al.*, 1988; Watanabe and Imamura, 2002; Akond and Watanabe, 2005; Akond *et al.*, 2008). Indeed, for both *T. petropavlovskyi* and ‘Arrancada’ the causal genetic locus for long glumes was mapped to chromosome 7A, supporting the hypothesis of a shared origin with *T. polonicum* (Watanabe and Imamura, 2002; Watanabe *et al.*, 2004).

The spatial and temporal expression of MADS-box transcription factors determine floral organ identity and developmental phase transitions in plants. The *Tunicate1* mutant of maize (*Zea mays*), known as pod corn, exhibits highly elongated leaf-like glumes that cover the kernels. Genetic

studies identified the causal gene as *Zea mays MADS19* (*ZMM19*), a member of the *short vegetative phase* (*SVP*) gene family of MADS-box transcription factors. A rearrangement in the promoter region of *ZMM19* causes its ectopic expression, which leads to the dosage-dependent phenotype (Han *et al.*, 2012; Wingen *et al.*, 2012). Ectopic expression of *ZMM19* in *Arabidopsis thaliana* leads to enlarged sepals, suggesting a conserved mechanism (Wingen *et al.*, 2012).

Spikelet morphology and organ size are tightly correlated with final grain weight in wheat (Millet, 1986). Despite their importance, we have relatively little understanding of the genes controlling spikelet and floral organ size in wheat. Here, we characterised the *P1* locus of *T. polonicum*, which has pleiotropic effects on glume, floral organ, and grain size. We show that the *P1* long-glume phenotype is due to the ectopic expression of *VRT-A2*, a *SVP* MADS-box transcription factor. The higher and ectopic expression of *VRT-A2* is due to a sequence substitution in the first intron, which defines *T. polonicum* as a subspecies. Expression levels of *VRT-A2* affect glume, grain, and floral organ length in a dosage-dependent manner.

Results

The long-glume *T. polonicum* *P1* allele enhances grain weight through longer grains

To evaluate the performance of the *T. polonicum* *P1* allele (hereafter called *P1^{POL}*) we developed BC₄ and BC₆ near isogenic lines (NILs) by crossing *T. polonicum* accession 1100002 to the hexaploid spring wheat cultivar Paragon (Table 1, Figure 1B). We verified the isogenic status of these lines using the Breeders' 35K Axiom Array (Supplementary Figure S1)(Allen *et al.*, 2017) and assessed the *P1^{POL}* and wildtype (*P1^{WT}*) NILs in the field over multiple years and environments. The *P1^{POL}* NILs had longer glumes and lemmas than wildtype Paragon NILs (Figure 1B) and were on average 6 cm taller due to an increase in peduncle (final internode) and spike lengths (1.6 cm; *P* < 0.01, Table 1; Supplementary Table S1-S3; Supplementary Figure S2). The *P1^{POL}* NILs also flowered on average 0.8 days later (*P* < 0.001) than the wildtype NILs. We observed consistent positive effects on thousand grain weight in *P1^{POL}* (TGW; 5.5%; *P* < 0.001), which were driven by significant increases in grain length (5.0%; *P* < 0.001), but not grain width (Table 1, Supplementary Table S1 and S4). The increase in grain length resulted in an increased grain volume (10.7%; *P* = 0.001) as determined by CT scans of a single year of field samples (Figure 1C, Supplementary Table S4). The increased TGW in *P1^{POL}* NILs also translated into a significant increase in hectolitre weight (HLW) in 4 out of 5 environments (2.3%; *P* < 0.01). Final yield, however, was not significantly different between NILs despite the increase in TGW (Table 1, Supplementary Table S1).

Table 1: Phenotypic effects of PI^{POL} allele in Paragon NILs. PI^{POL} effect is the percentage difference (except height and spike length in cm; heading date in days) between the PI^{WT} and the PI^{POL} NILs. The P value of the ANOVA main effect is presented, apart from grain width, which had a significant interaction across environments (simple effects and detailed breakdown in Supplementary Table S1). Values represent means of six field experiments (except spike length $n=4$).

Allele	Height (cm)	Spike Length (cm)	Heading date (days)	HLW (kg/hl)	TGW (g)	Grain Width (mm)	Grain Length (mm)	Yield (kg/plot)
PI^{POL}	90.6	13.2	218.5	77.2	46.8	3.584	6.757	5.237
PI^{WT}	84.6	11.6	217.7	75.5	44.4	3.589	6.438	5.212
PI^{POL} effect	6.0	1.6	0.8	2.3%	5.5%	-0.1%	5.0%	0.5%
P value	2.0E-13	0.005	4.4E-07	0.009 *	6.9E-06	Interact.	< 2.2e-16	NS

* PI^{POL} NIL was significant in 5 out of 6 environments.

PI^{POL} enhances grain size in florets 1 and 2 through an increase in cell length

We conducted more in-depth phenotyping to identify the first timepoint during grain development in which differences in grain length are established between PI NILs. We dissected and measured field-grown grain samples from florets 1 and 2 of five central spikelets from PI^{WT} and PI^{POL} NILs at six timepoints during grain development (Figure 1D; second year data in Supplementary Figure S3). We did not detect consistent differences in ovary length before and at anthesis nor in grain length 7 days post anthesis (dpa). However, at 14 dpa, grains from PI^{POL} NILs were 3.4 % longer than grains from PI^{WT} NILs ($P < 0.05$) (Supplementary Table S5). The increased grain length in PI^{POL} NILs was maintained at 21 and 28 dpa (7.0 and 6.2% longer grains than PI^{WT} , respectively; $P < 0.002$) (Supplementary Table S5). These results, consistent in two independent field seasons (Supplementary Figure S3), suggest that the difference in grain length between PI NILs is established during mid-grain filling.

We next measured the size (length, width, and area) of glumes, floral organs (lemma and palea), and grains across spikes and spikelets of PI^{POL} and PI^{WT} NILs using the same field-grown samples as above. Having already established that the main effect of the PI^{POL} allele was to increase organ length, we focus on it in the following paragraph (all data, including width and area measurements, in Supplementary Tables S2-S3, Supplementary Figures S4-S5). The PI^{POL} allele significantly increased glume length (37%; $P < 0.001$) with respect to the wildtype NILs; this effect was consistent and independent of spikelet position across the spike (Figure 1E). However, we detected a significant gradient in the effect of the PI^{POL} allele across the florets within each spikelet. The largest and most significant PI^{POL} effects on lemma length were observed in florets 1 and 2 (28.6%

and 19.8%, respectively; $P < 0.001$), whereas the effect was reduced in floret 3 (+5.8%; $P < 0.001$) and was non-significant in floret 4 (Figure 1F, Supplementary Table S3). This gradient in lemma length within spikelets was maintained across all positions along the spike. A very similar gradient within spikelets was also identified for grain length, with PI^{POL} NILs having significantly longer grains than PI^{WT} NILs in florets 1 and 2 (+4.1% and +6.7%, respectively; $P < 0.001$), and non-significant differences in grain length in florets 3 (+0.4%; $P = 0.37$) and 4 (+0.1%; $P = 0.92$) (Figure 1F). Minor effects of the PI^{POL} allele on palea length also followed this spikelet gradient (+2.5% in floret 1 to -3.6% in floret 4; Supplementary Table S3, Supplementary Figure S5). These results suggest that the increases in glume, lemma, and grain length conferred by the PI^{POL} allele are consistent along the spike, but that the positive effects on lemma and grain length follow a basipetal gradient from basal to apical florets within individual spikelets.

To further investigate the differences in grain length between PI NILs, we used scanning electron microscopy to image and measure pericarp cell size of PI^{WT} and PI^{POL} grains. We selected grains from florets 2 and 4 of central spikelets and imaged the base, centre, and distal end of each grain (Supplementary Figure S6A). We found a significant 12.9 % increase ($P < 0.05$) in pericarp cell length in floret 2 grains of PI^{POL} NILs relative to PI^{WT} NILs (Figure 1G). This difference in cell length was present only in the central portion of the grain, while cell size was similar between NILs at the base and distal end of the grain (Supplementary Table S6, Supplementary Figure S6). For floret 4, there were no differences in pericarp cell size between the NILs at each of the three positions examined across the grain (Figure 1G, Supplementary Table S6, Supplementary Figure S6). Given the maternal origin of the pericarp, these results are consistent with the PI^{POL} grain length effect being maternally inherited as first proposed by Engledow (1920). Taken together, these results suggest that PI^{POL} enhances grain size in basal florets through an increase in cell length in the centre of the grain, whereas grains of floret 3 and 4 are indistinguishable from the wildtype NILs, both macro- and microscopically.

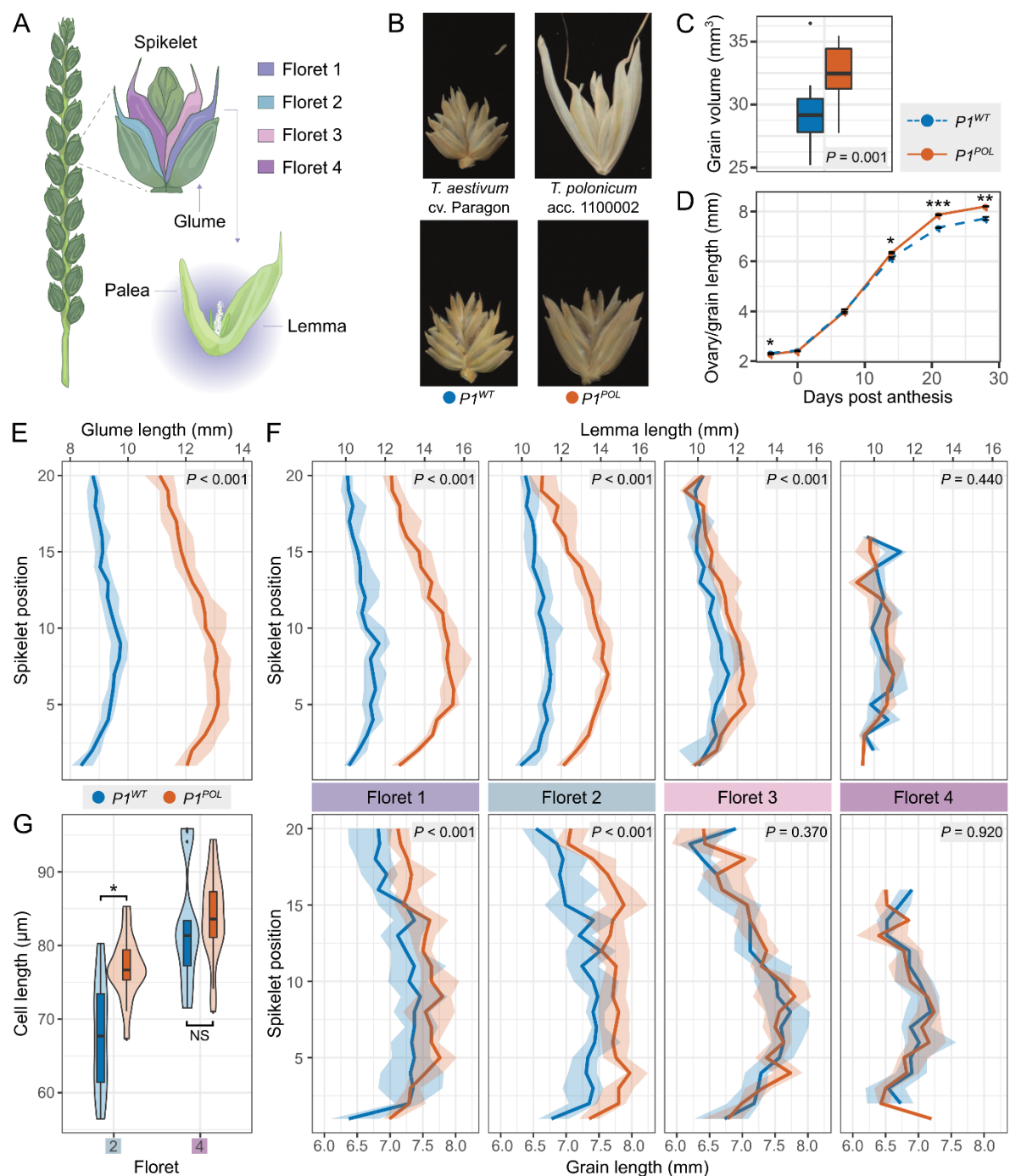


Figure 1. Phenotypic effects of *P1* in near-isogenic lines (NILs)

(A) Drawing of a wheat spike, with a close-up of an individual spikelet. The first four florets on the spikelet are colour coded. A close-up of an open floret depicts its two enveloping sheathing structures (lemma and palea). (B) Spikelets of the parental hexaploid bread wheat cultivar ‘Paragon’ and tetraploid *T. polonicum* accession 11000002, and the *P1*^{WT} and *P1*^{POL} NILs. (C) Grain volume was measured using a CT-scanner to image field-grown spikes of the two NILs (n=15). (D) Timecourse tracking ovary/grain length development in field-grown *P1*^{WT} and *P1*^{POL} NILs (n=50). (E) Glume length along spikes of *P1*^{WT} and *P1*^{POL} NILs; positions are numbered from basal to apical spikelets (n=15 spikes). (F) Lemma and grain length at each floret position along *P1*^{WT} and *P1*^{POL} NILs spikes. Spikelet positions as in E (n= 15 spikes). In (E) and (F) bold line represents the median value, ribbon represents the interquartile range. (G) Pericarp cell length from middle sections of grains from floret 2 and floret 4 for the *P1*^{WT} and *P1*^{POL} NILs (n= 18 grains). See Supplementary Table S6 for additional measurements. Error bars represent mean ± SEM. *, *P* < 0.05; **, *P* < 0.01; ***, *P* < 0.001.

***PI* maps to a 50 kb interval on chromosome 7A containing a single candidate gene**

To map the *PI* locus, we used BC₄ and BC₆ recombinant lines derived from the NILs described above. We initially phenotyped 17 BC₄F₃ homozygous recombinant lines between markers *S1* and *S9* for glume length and mapped the *PI* locus between markers *S2* (125,260,256 bp) and *S7* (150,240,183 bp) (Figure 2A, Supplementary Table S7). Heterozygous individuals across the interval had glumes of intermediate length between the homozygous wildtype and *PI*^{POL} lines, consistent with a semi-dominant mode of action of *PI* (Biffen, 1905; Engledow, 1920; Okamoto and Takumi, 2013). To further define the *PI* interval, we identified an additional 64 homozygous BC₆F₂ recombinants between markers *S2* and *S10*, which were genotyped with a further 21 markers (Figure 2B, Supplementary Table S8). The long-glume phenotype, alongside plant height, spike length, grain length, and thousand grain weight, mapped between markers *S15* and *S19*, spanning a 50,338 bp interval (Figure 2C, Supplementary Table S8-S9). The complete linkage of the 50.3 kbp region with these multiple phenotypes suggests that they are all pleiotropic effects of the *PI* locus.

We identified two gene models based on the RefSeqv1.1 annotation within the *PI* interval: *TraesCS7A02G175100* and *TraesCS7A02G175200*. The flanking marker *S15* resided within the last intron of *TraesCS7A02G175100* and no additional SNPs were detected in the last exon of this gene between *PI*^{WT} and *PI*^{POL} NILs. Manual annotation of the 50.3 kbp *PI* interval in the RefSeqv1.0 assembly (and an additional 14 hexaploid and tetraploid cultivars) identified 38,261 bp as repetitive sequences, and no additional gene apart from *TraesCS7A02G175200* (Figure 2D, Supplementary Figure S7A). This suggested *TraesCS7A02G175200* as the sole candidate gene for *PI*.

TraesCS7A02G175200 encodes a member of the MADS-box gene family previously named *VEGETATIVE TO REPRODUCTIVE TRANSITION 2* (*VRT2*) in wheat (Kane *et al.*, 2005). *VRT2*, as well as its homolog *TaSVPI*, are the closest wheat orthologs of *AtSVP* in *Arabidopsis thaliana* and *OsMADS55* in rice (Supplementary Figure S8). Using publicly available RNA-Seq data, we verified the exon-intron structure of *TraesCS7A02G175200.1* (Supplementary Figure S7B). We sequenced the gene in the *PI*^{POL} NIL from 2299 bp upstream of the ATG to marker *S19* (1857 bp downstream of the STOP codon; 9747 bp total including all exons and introns). Compared to the RefSeqv1.0 assembly, we only found a single polymorphism; a 563-bp sequence in the RefSeqv1.0 assembly that was substituted for a 160-bp sequence in *PI*^{POL} (Figure 2E, Supplementary Table S10).

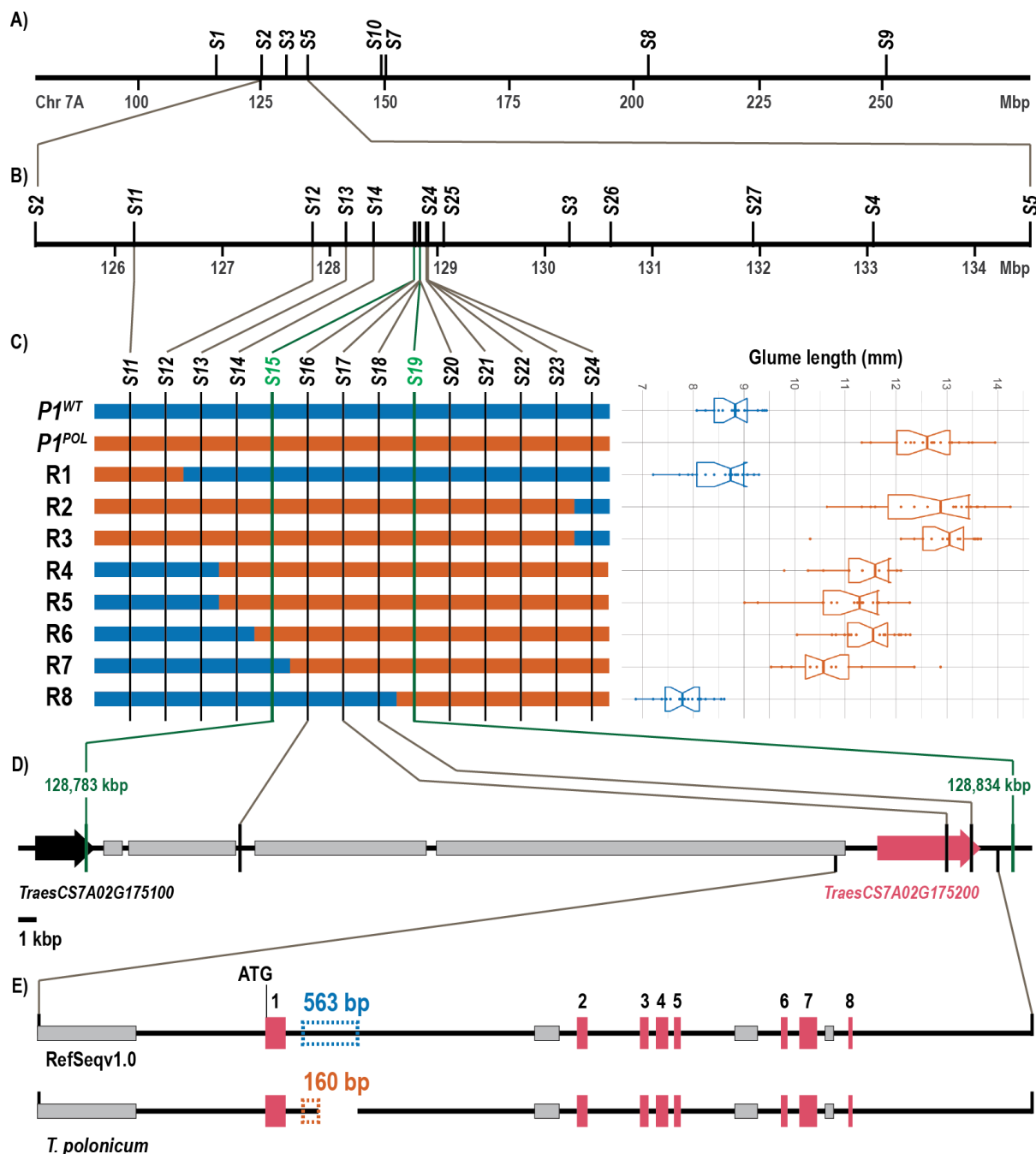


Figure 2. Map-based cloning of the *P1* locus reveals *VRT-A2* as the single candidate gene
(A) Initial mapping in 17 BC₄F₂ recombinants mapped *P1* between markers S2 and S7 (~25 Mbp interval). **(B)** Subsequently, *P1* was mapped between markers S2 and S10 using an additional 64 BC₆F₂ recombinant lines. **(C)** Graphical genotype of eight critical recombinants between markers S12 and S24 (~1 Mbp interval; marker distance not drawn to scale). Based on the phenotypic evaluation of glume length, we mapped *P1* to a 50.3 kbp interval between markers S15 and S19. **(D)** The 50.3 kbp interval encompasses the last exon of *Traes7A02G175100* (black arrow), multiple repetitive elements (grey rectangles) and *Traes7A02G175200* (red arrow). **(E)** We identified a single polymorphism between Chinese Spring (RefSeqv1.0) and *T. polonicum* in a ~10 kbp interval encompassing *Traes7A02G175200*. A 563-bp sequence in RefSeqv1.0 was substituted by a 160-bp sequence in *T. polonicum*.

The 160-bp intron-1 sequence substitution in *VRT-A2* is completely linked with the long-glume phenotype in tetraploid and hexaploid wheat accessions

We determined the allelic status of the *VRT-A2* intron-1 sequence substitution in a wheat diversity panel. We first screened 187 accessions with wildtype glume length including tetraploid emmer wheat *T. dicoccoides* (n=70), hexaploid wheat landraces (n=103), and 16 sequenced wheat cultivars. We found that all 189 accessions carried the wildtype 563-bp sequence in intron 1 and none had the 160-bp sequence substitution found in *PI^{POL}* (Supplementary Table S11). We next screened 23 accessions of tetraploid *T. polonicum* (all with long glumes) from 15 different countries to determine the intron-1 sequence of *VRT-A2*. All 23 *T. polonicum* accessions carried the identical 160-bp substitution in intron 1 as the *PI^{POL}* allele (Figure 3A, B, Supplementary Table S12). These results suggest that the *VRT-A2* 160-bp sequence substitution in intron 1 is unique to *T. polonicum*.

We then examined accessions from two types of hexaploid wheat with long-glumes that have been postulated to be the product of independent hybridisation between *T. polonicum* and hexaploid landraces in China (*T. petropavlovskyi*) and Portugal ('Arrancada' group) (Chen *et al.*, 1985; Chen *et al.*, 1988; Watanabe and Imamura, 2002; Akond and Watanabe, 2005; Akond *et al.*, 2008) (Figure 3A, C). All 9 accessions of *T. petropavlovskyi* (n=2) and the 'Arrancada' landraces (n=7) carried the same 160-bp substitution in *VRT-A2* intron 1 as that found in *T. polonicum* (Supplementary Tables S12). We fully sequenced the allele (5591 bp) from six *T. polonicum*, two *T. petropavlovskyi*, and four 'Arrancada' accessions (Supplementary Table S12) and obtained 100% identical sequences from these twelve long-glumed accessions. Using the markers developed for mapping *P1*, we found that our two *T. petropavlovskyi* accessions shared a common haplotype, whereas the seven 'Arrancada' accessions also shared a common, albeit distinct, haplotype from that in *T. petropavlovskyi* (Supplementary Table S13). Conversely, in accessions with normal-sized glumes, we identified multiple haplotypes within *VRT-A2* (all with the 563-bp intron-1 sequence) and also across the wider physical interval (Supplementary Tables S10, S13). These results, alongside the absence of the 160-bp substitution in wild emmer and hexaploid landraces, provide evidence that the 563-bp intron-1 sequence in *VRT-A2* is ancestral.

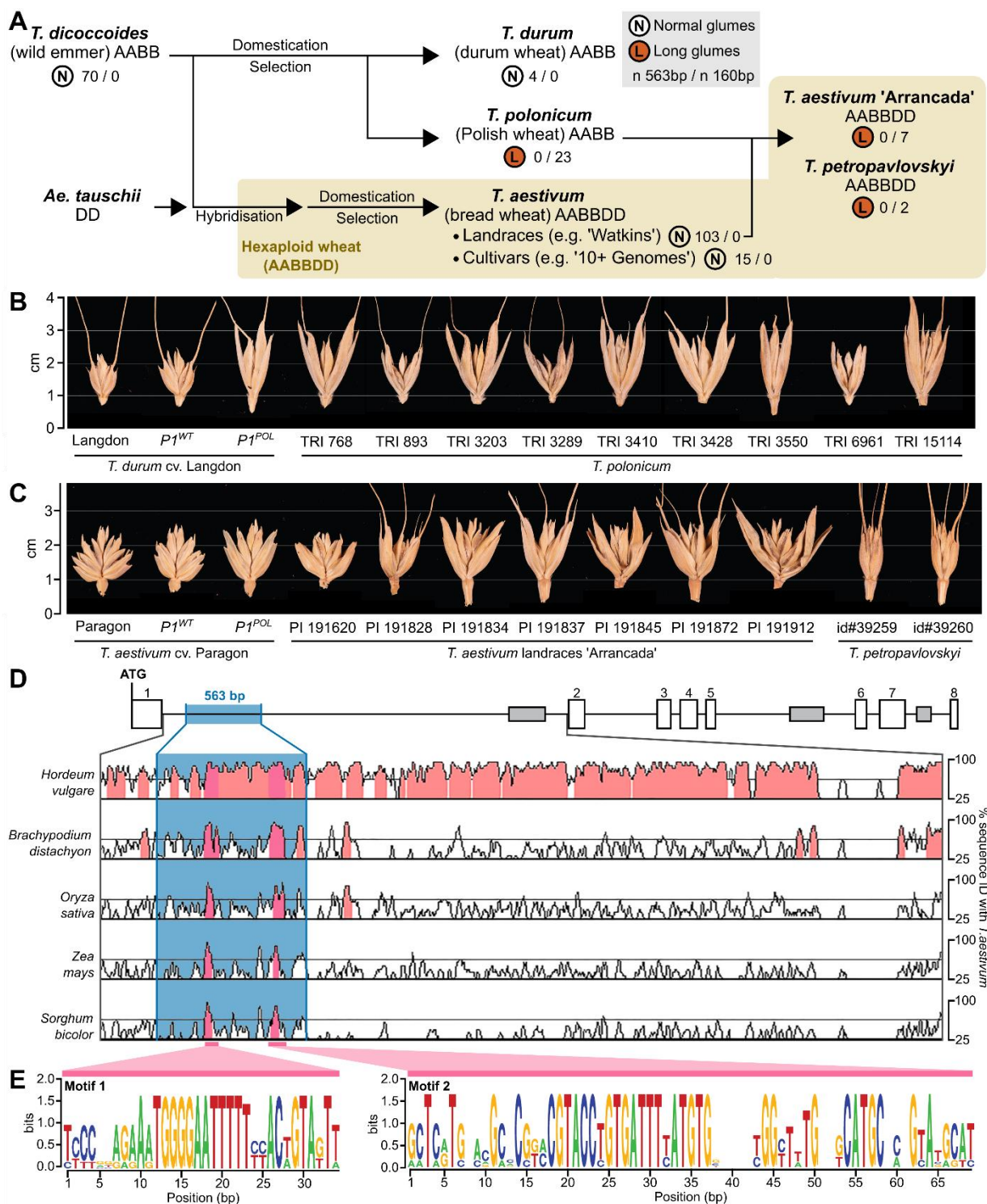


Figure 3. Natural variation of *P1* indicates a single mutation event that led to the loss of evolutionary conserved motifs

(A) Simplified diagram depicting the evolution and domestication of tetraploid and hexaploid wheat (tan shaded area). The glume phenotype for each species and set of accessions is indicated by the letter N (normal) or L (long) enclosed in a circle. Beside this classification, the number of accessions that carry the wildtype 563-bp intron 1 or the 160-bp intron 1 *VRT-A2* allele is shown. *T. polonicum* hybridised with hexaploid landraces in China and Portugal, giving rise to *T. petropavlovskiyi* and the 'Arrancada' landrace group, respectively, both of which exhibit long glumes and carry the 160-bp intron 1 *VRT-A2* allele. (B) Spikelets of tetraploid wheat including *P1* NILs in the tetraploid cultivar 'Langdon' and nine accession of *T. polonicum*. (C) Comparison of spikelets of hexaploid wheat including *P1* NILs in the hexaploid cultivar 'Paragon', seven accession

from the ‘Arrancada’ landrace group and two accession of *T. petropavlovskiyi*. (D) Phylogenetic shadowing using mVISTA of *VRT-A2* intron 1 with pairwise alignments of *T. aestivum* with barley (*Hordeum vulgare*), *Brachypodium distachyon*, rice (*Oryza sativa*), maize (*Zea mays*), and sorghum (*Sorghum bicolor*). The Y-axis represents percentage sequence similarity. Two conserved peaks (dark pink) were identified within the 563-bp sequence (blue box) that is absent in *T. polonicum*. (E) Sequence of the two conserved motifs that maintain an >80% similarity over a 20 bp sliding window across the species described in D.

The wildtype 563-bp intron-1 sequence of *VRT-A2* is highly conserved across Poaceae

We compared the entire wildtype intron-1 sequence of *VRT-A2* with orthologous Poaceae sequences from barley (*Hordeum vulgare*), *Brachypodium distachyon*, rice (*Oryza sativa*), maize (*Zea mays*), and sorghum (*Sorghum bicolor*). Phylogenetic shadowing using mVISTA (Mayor *et al.*, 2000; Frazer *et al.*, 2004) revealed two highly conserved regions across Poaceae (>85% sequence id, minimum 20 bp), both of which are missing from the 160-bp substitution found in the *PI^{POL}* allele (Figure 3D). We further examined these two regions (see Methods) and identified broadly conserved sequences of 34 and 69 bp in length, hereafter referred to as ‘Motif 1’ and ‘Motif 2’ respectively (Figure 3E). Within them, both motifs contain highly conserved sequences of 16 and 20 bp, respectively (Supplementary Data Set S1). We searched for putative transcription factor binding sites within Motifs 1 and 2 using three online databases (PlantPan3.0, PlantRegMap, and MEME, see Methods). We found two significant hits (both $P < 0.001$ and $q < 0.001$) for Motif 1 encoding members of the LATERAL ORGAN BOUNDARIES-DOMAIN (LBD) family (Supplementary Data Set S2). For Motif 2, we found 17 significant hits (all $P < 0.001$ and $q < 0.05$) encoding members of the LBD, Basic Leucine Zipper (bZIP), B3, and GLABROUS1 enhancer-binding protein (GeBP) families (Supplementary Data Set S2). Given the highly conserved nature of motifs within the 563-bp intron-1 sequence across the investigated Poaceae (~60 million years divergence time; (Charles *et al.*, 2009; Reineke *et al.*, 2011)) and the identification of putative transcription factor binding sites, we hypothesise that this intron-1 sequence plays a regulatory role in the expression profile of *VRT-A2*.

***VRT-A2* is expressed ectopically and more highly in *PI^{POL}* relative to *PI^{WT}* NILs**

To assess if the intron-1 sequence substitution affected the expression profile of *VRT-A2*, we determined its expression pattern in *PI^{WT}* and *PI^{POL}* NILs using qRT-PCR. We first examined expression levels in developing meristems of *PI^{WT}* NILS. Consistent with previous studies (Kane *et al.*, 2005; Kane *et al.*, 2007; Trevaskis *et al.*, 2007), we found a progressive decrease in *VRT-A2* expression from vegetative meristem (W1) to terminal spikelet stage (W4)(Figure 4A). We next examined expression in *PI^{POL}* NILs, which showed a five to 16-fold higher expression level of

VRT-A2 relative to the *PI^{WT}* NILs at all five timepoints investigated ($P < 0.05$; Figure 4A). An increased expression level of *VRT-A2* in *PI^{POL}* relative to *PI^{WT}* was also observed in leaves at the same developmental stages (six to 38-fold higher, $P < 0.05$) (Supplementary Table S14). We next examined *VRT-A2* expression in developing glumes, lemmas, anthers, flag leaves, and grains at multiple developmental timepoints. In the wildtype NIL, expression was restricted to the flag leaves and anthers at anthesis (Figure 4B, Supplementary Table S14). We did not detect *VRT-A2* expression in glumes, lemmas, nor grains of *PI^{WT}* NILs at any timepoint (Figure 4B-D), consistent with publicly available RNA-Seq data of wildtype *VRT-A2* genotypes (Borrill *et al.*, 2016; Ramírez-González *et al.*, 2018). By contrast, *VRT-A2* expression was detected in all tissues and at all timepoints in *PI^{POL}*, including glumes, lemmas, and grains (Figure 4B-D).

Given the contrasting effects of the *PI^{POL}* allele on grain and lemma length between floret 1+2 and floret 4 (Figure 1F), we compared the *VRT-A2* ectopic expression in these samples. Across multiple tissues and timepoints (lemma, palea, pistil at anthesis; grains at 4, 10, and 20 days post anthesis) we found similar expression of *VRT-A2* in samples from florets 1+2 compared to floret 4 (Figure 4 C, D). We also investigated expression of the *VRT2* homoeologs (*TraesCS7B02G080300*, *TraesCS7D02G176700*), and that of the closely related ortholog *TaSVPI* (*TraesCS6A02G313800*, *TraesCS6B02G343900*, *TraesCS6D02G293200*) (Supplementary Figure S8). Across the same tissues and developmental time points as those described above, we did not detect any differences in expression between *PI^{WT}* and *PI^{POL}* NILs (Figure 4E). These results show that *VRT-A2* is expressed more highly and ectopically in *PI^{POL}* relative to *PI^{WT}* NILs across multiple tissues and timepoints. The ectopic expression does not extend to the homoeologs or closely related orthologs and is not restricted to those tissues in which we observed phenotypic differences between *PI^{WT}* and *PI^{POL}* NILs.

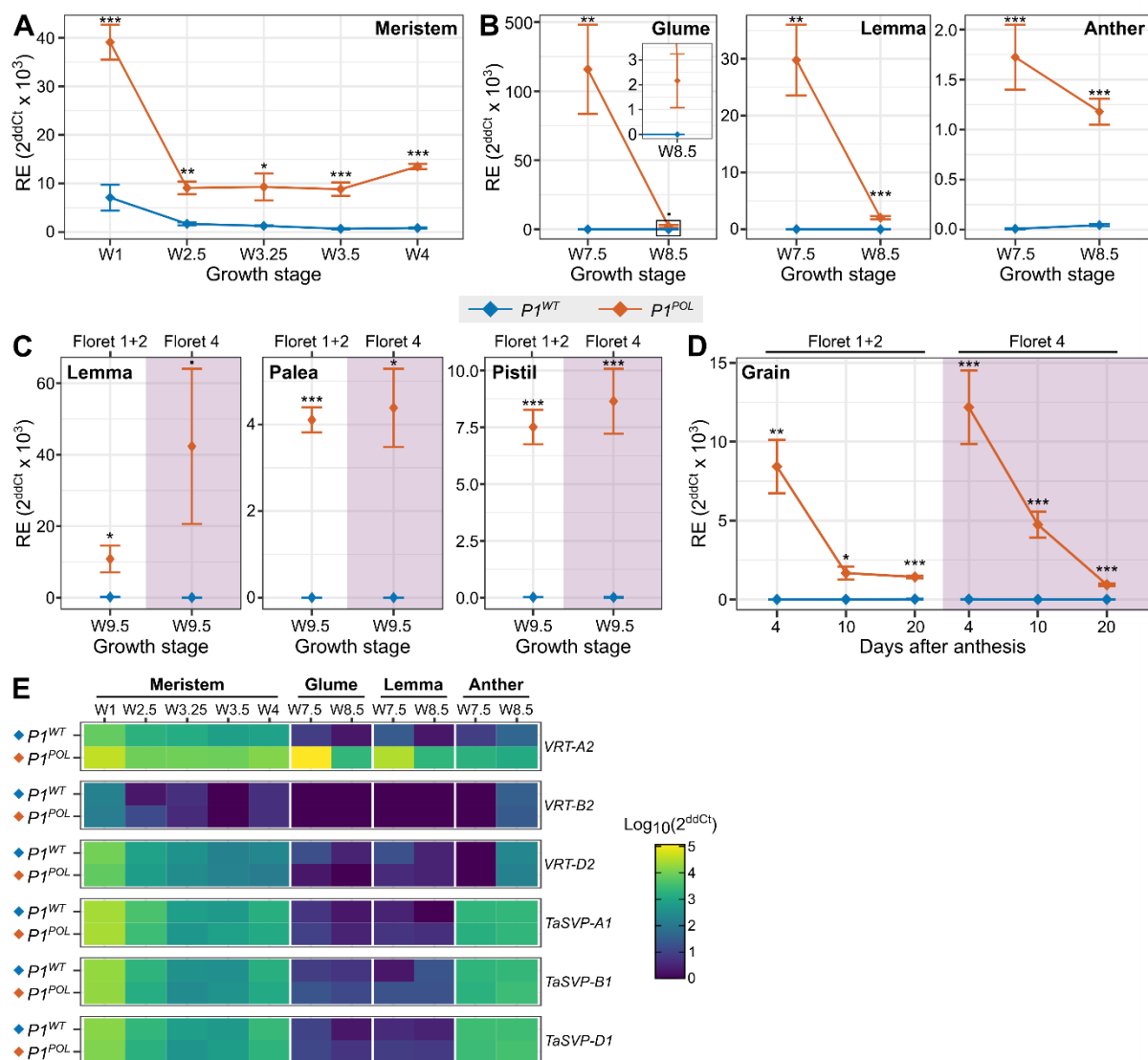


Figure 4. *VRT-A2* is more highly and ectopically expressed in $P1^{POL}$ relative to $P1^{WT}$ NILs
(A) Relative expression of *VRT-A2* in developing meristems of $P1^{WT}$ (blue) and $P1^{POL}$ (orange) NILs. Developmental stages based on Waddington scale (Waddington *et al.*, 1983); W1, vegetative meristem; W2.5, late double ridge stage; W3.25, lemma primordium stage; W3.5, floret primordium stage; W4, early terminal spikelet stage. **(B)** Relative expression of *VRT-A2* in glume, lemma (floret 1+2), and anther (floret 1+2) at W7.5 (spike in boot with stigmatic branches elongating) and W8.5 (spike just in boot with stigmatic branches forming a tangled mess). **(C)** Relative expression of *VRT-A2* in lemma, palea, and pistil just before anthesis (W9.5) in florets 1+2 (white background) and floret 4 (pink background). Note that for Panel C and D the growth stage is based on florets 1+2; floret 4 tissues will be at a slightly less mature developmental stage. **(D)** Relative expression of *VRT-A2* in grains from florets 1+2 as well as floret 4 at 4, 10, and 20 days post anthesis. **(E)** Heatmap showing \log_{10} scaled expression in $P1^{WT}$ and $P1^{POL}$ NILs for the three *VRT2* and *TaSVP1* homoeologs in tissues and developmental stages shown in panels A and B (Supplementary Table S14). Error bars are mean \pm SEM. *, $P < 0.05$; **, $P < 0.01$; ***, $P < 0.001$.

Ectopic expression of *VRT-A2* leads to phenotypic effects in a dosage dependent manner

We next tested whether the observed changes in *VRT-A2* expression patterns in *PI^{POL}* NILs are causal for the *T. polonicum* long-glume phenotype. We transformed the hexaploid accession ‘Fielder’ (normal glume phenotype) using the genomic *T. polonicum* *VRT-A2* allele (5591 bp), including 2299 bp upstream of the ATG, all coding and intron sequences, as well as 1000 bp downstream of the termination codon. We obtained 14 independent T₀ lines, which were classified based on the transgene copy number. No transgene was detected for five lines (zero copy number), three lines carried 1 or 2 copies (low copy number), three lines carried 4 to 5 copies (medium copy number), and three lines carried 9 to 35 copies (high copy number) (Figure 5A, Supplementary Tables S15-S17).

We collected tissue from flag leaves, glumes, and grains at 21 dpa from all 14 plants to measure expression levels of *VRT2* homoeologs (Supplementary Table S15). We detected expression of *VRT-A2* in flag leaves of all 14 transformed lines, including the zero copy number lines, similar to that observed in *PI^{WT}*. In glume and grain tissue, *VRT-A2* expression was extremely low or not detected in the zero copy number lines, consistent with the *PI^{WT}* NILs (Figure 4), whereas we detected expression in all lines with at least one copy of the transgene. In all tissues, *VRT-A2* expression scaled with copy number. As seen in the NILs, we did not detect differences in expression of the B- and D-homoeologs among transgenic lines (Supplementary Table S15). We dissected all spikelets from two spikes of each of the 14 T₀ lines for morphological characterisation. We compared spike length and glume length, as well as lemma, palea, and grain length from florets 1 to 4 among the four categories of copy number lines (Figure 5A-C; Supplementary Table S16). Overall, we identified significant differences between the zero copy lines (N = 5) and the transgenic lines (low, medium, and high; N = 9) for glume, lemma, palea, and grain length (all *P* < 0.05; Supplementary Table S16). These differences were largest in glumes (42%) and lemmas (26%), whereas paleae showed the smallest effect (6.6%; Figure 5B, C; Supplementary Table S16).

Having established the overall positive effects of the *T. polonicum* *VRT-A2* transgene on these traits, we next evaluated the magnitude of the phenotypic effects among the four categories of copy number lines. Due to the relatively small sample size for each category (N=3 to 5 T₀ plants), we did not detect significant differences between zero copy number lines and low copy number lines for any of the traits, although glume length increased by 14.1% (*P* < 0.08). However, we did detect significant effects for glume length (19.0%), palea length (5.9%) and grain length (9.6%) in medium copy number lines (all *P* < 0.05). These effects increased in magnitude and significance in

high copy number lines, which showed a highly significant increase of 93% in glume length, 58% in lemma length, 13% in palea length, and 14% in grain length with respect to the zero copy number lines (all $P < 0.002$; Supplementary Table S16). While spike length was increased in both low and medium copy number lines (3% and 14% respectively), it was only significantly increased in high copy number lines with a 51% increase compared to zero copy number lines ($P < 0.01$). Consistent with what we observed in the NILs, we again saw a gradient in the phenotypic effects from floret 1 to floret 4. This basipetal gradient was most obvious in the medium and high copy number lines. For example, floret 1 lemma and grain length increased by 105% and 19%, respectively, in high copy number lines, whereas in floret 4 both traits ‘only’ increased by 11% (Supplementary Table S16).

We further analysed the phenotypic data to relate it to the expression of *VRT-A2* in the different transgenic lines. *VRT-A2* expression correlated highly and significantly with several phenotypic traits, independent of the tissue examined for expression. For example *VRT-A2* expression levels in the glume correlated strongly with spike length ($R^2 = 0.76$, $P < 0.0001$) and glume length ($R^2 = 0.92$, $P < 0.0001$) (Figure 5D), as well as with lemma, palea, and grain length in floret 1 (all $R^2 > 0.81$; all $P < 0.0001$) (Supplementary Table S17). Similar to the gradient in phenotypic effects across florets detailed above, these correlations were strongest and most significant in floret 1 and floret 2 ($R^2 > 0.64$), remained significant for floret 3 phenotypes ($R^2 \geq 0.41$), and were less significant for floret 4 phenotypes (Supplementary Table S17). The multiple phenotypes of the medium and high copy transgenic lines recreate, in a dosage dependent manner, the effects seen in the *PI^{POL}* NIL, providing further evidence that *VRT-A2* is the causal gene underlying the *T. polonicum* *PI* locus.

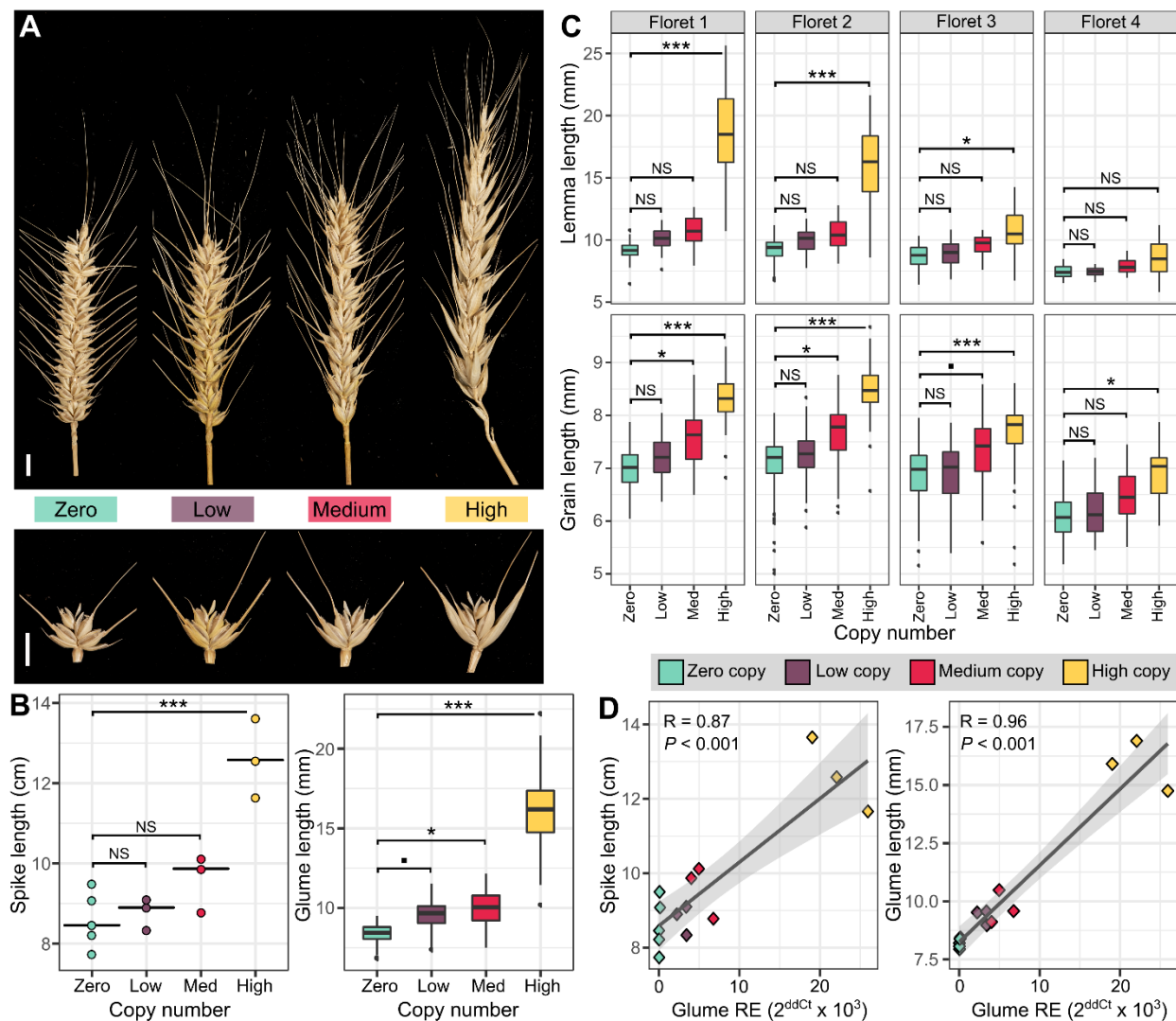


Figure 5. Increased and ectopic *VRT-A2* expression elicits phenotypic effects in a dosage dependent manner

(A) Comparison of spikes and spikelets of zero, low (1-2), medium (3-4), and high (9-35) copy number lines (left to right). Notably, spike length increases with copy number, as does glume length. Scale bar = 1 cm. (B) Dot and box plots depicting the variation of spike (left) and glume (right) length, respectively, from two tillers of zero (cyan), low (purple), medium (red), and high (yellow) copy number lines. Horizontal lines represent the median. (C) Box plots depicting lemma and grain length for florets 1, 2, 3, and 4 for zero (cyan), low (purple), medium (red), and high (yellow) copy number lines. (D) Pearson correlations between *VRT-A2* relative expression in the glume at 21 dpa and spike length (left), and glume length (right). Relative expression shown as $2^{\text{ddCt}} \times 10^3$. Regression (Dark grey line) and 95% confidence interval (light grey shading) are shown. Data points are coloured according to copy number. Statistical classifications in (B) and (C) are based on Dunnett tests against the zero copy number lines. ■, $P < 0.10$; *, $P < 0.05$; **, $P < 0.01$; ***, $P < 0.001$.

Discussion

The first formal classification of wheat was compiled by Linnaeus in 1753 and was based on discernible characteristics such as phenology, spike architecture, and glume morphology. With its characteristic long glumes *T. polonicum* is a standout *Triticum* species. Despite this, the first mention of *T. polonicum* only dates back to 1687 (Percival, 1921). *T. polonicum* was instrumental in the study of early geneticists who showed that measurable quantitative traits, such as glume length, were also inherited according to the same laws of qualitative traits postulated by Mendel (Biffen, 1905; Engledow, 1920). However, despite first being described genetically over a century ago, the gene underlying the *PI* locus remained unknown.

Here, we show that the gene underlying the long-glume *PI* locus of *T. polonicum* is *VRT-A2*, a member of the *SVP* family of MADS-box transcription factors. We mapped multiple phenotypes associated with *PI*, including glume length, grain length, spike length, grain weight, and plant height to the same physical interval that included *VRT-A2* as the single candidate gene. For grains, we further showed that the increase in length is likely a result of increased cell length. We identified a sequence substitution in the first intron of *VRT-A2* in which a 563-bp wildtype sequence was replaced by a 160-bp fragment in *T. polonicum*. Using diverse germplasm, we showed that this 160-bp fragment is only present in tetraploid *T. polonicum* accessions, or in hexaploid wheat germplasm with long glumes. Our results provide strong evidence that these hexaploid wheat accessions with long-glumes, namely *T. petropavlovskyi* and the ‘Arrancada’ accessions, are the outcome of introgressions between *T. polonicum* and hexaploid wheat (Chen *et al.*, 1985; Chen *et al.*, 1988; Watanabe and Imamura, 2002; Akond and Watanabe, 2005; Akond *et al.*, 2008). The lack of *VRT-A2* sequence variation among lines with the *PI^{POL}* allele, coupled with the absence of the *PI^{POL}* allele among ancestral wheat types (e.g. wild emmer, Watkins landraces) suggests a single and recent origin for the *PI^{POL}* allele. We propose that a single mutation event in the ancestral *VRT-A2* intron-1 sequence gave rise to the 160-bp sequence substitution within the domesticated tetraploid gene pool. This mutation was later introduced into hexaploid wheat via natural hybridizations resulting in hexaploid accessions with long-glumes. These results, together with the complete linkage of this 160-bp sequence substitution with the long-glume phenotype, suggest that the intron-1 mutation in *VRT-A2* is the *T. polonicum* species defining polymorphism.

We observed that *VRT-A2* was expressed to a higher degree in *PI^{POL}* compared to wildtype in all tested tissues (e.g. developing spikelets, leaves, and anthers). Furthermore, we observed ectopic *VRT-A2* expression in *PI^{POL}* tissues that have no detectable expression in wildtype lines (e.g.

glumes and grains). These expression profiles were also found in transgenic lines that carry the *PI^{POL}* allele, which includes the 160-bp intron-1 sequence. In these transgenic lines, we found a linear relationship between expression levels and multiple phenotypic traits ($R^2 = 0.76$ for spike length, $R^2 = 0.92$ for glume length; $R^2 = 0.88$ for lemma length; $R^2 = 0.81$ for grain length; $R^2 = 0.83$ for palea length; all $P < 0.001$). The NIL and transgenic data also suggest that outer organs, including glumes and lemmas, are more responsive to changes in *VRT-A2* expression levels than inner organs such as paleae and carpels. Our results suggest that ectopic and higher expression of *VRT-A2* leads to multiple phenotypic effects, including the glume, lemma, and grain length phenotypes, in a dosage dependent manner in polyploid wheat.

In the *PI^{POL}* NIL, we detected ectopic expression of *VRT-A2* in tissues that do not show morphological changes (e.g. lemma and grains from floret 4) nor differences in pericarp cell size (e.g. grains from floret 4). Similarly, we only detected an increase in length in paleae from floret 1, but not subsequent florets. This is recapitulated in the transgenic lines with medium copy number of the transgene (Supplementary Table S16). In contrast, the lines with high copy number show significant increases in lemma length ($P < 0.02$) and grain length ($P \leq 0.02$) within floret 3 and 4, respectively. Similarly, palea length is only significantly different in floret 1 in the *PI^{POL}* NIL, whereas paleae are longer up until floret 3 in the high copy number transgenic lines. This suggests that increasing expression levels of *VRT-A2* are necessary to alter organ length in subsequent florets and across different organs. The strongest effects are visible in the basal florets of the spikelets, and only transgenic lines with medium or high copy number exhibit changes in organ length in apical florets, consistent with a basipetal gradient that determines organ length. Both lemma and palea, and the resulting grain, respond to this gradient, although the magnitude of the phenotypic effects (with respect to wildtype or zero copy lines) is stronger in lemmas than in paleae.

A possible explanation for these results is the sequential formation of these organs during spikelet and floral development together with the fact that MADS-box genes act in sequential manner as part of protein complexes. In the wildtype, *VRT2* expression is strongly downregulated during the transition from vegetative meristem to the double ridge stage, presumably to allow floral transition from vegetative to spikelet and floret meristems (Trevaskis *et al.*, 2007). Thus, normal transition into floral meristems takes place under decreasing SVP levels and increasing levels of A-class and E-class MADS-box proteins, among others. However, overexpression of *SVP* genes in barley (Trevaskis *et al.*, 2007) can affect this balance and lead to a delay or a reversion of this vegetative to reproductive transition. Thus, outer and early established organs (e.g. glumes and lemmas) are kept for a longer period in a less differentiated stage, while later developing/differentiating organs (e.g.

paleae) are not or only slightly affected. Alternatively, VRT2 interacting partners could be expressed in a basipetal gradient, with high abundance in basal organs and low or no abundance in apical florets. A combination of these two explanations is also possible.

Our results are reminiscent of the pod corn phenotype observed in maize *Tunicate1* (*Tu1*) mutants, in which the grains (kernels) are completely enclosed by elongated glumes. Similar to *PI*, the mutant *Tu1* phenotype is caused by the ectopic expression of *ZMM19*, the maize *TaSVPI* homolog and a closely related ortholog of wheat *VRT2*, in the developing maize inflorescence (Han *et al.*, 2012; Wingen *et al.*, 2012). The ectopic expression of *ZMM19*, however, is due to a duplication and rearrangement in the promoter region, whereas our results indicate that the intron-1 sequence plays a key regulatory role in the expression profile of *VRT-A2*.

Numerous MADS-box genes have been shown to contain regulatory sequences within their first introns, including *FLC* in *Arabidopsis* (Sung *et al.*, 2006) and *VRN1* in wheat (reviewed in Distelfeld *et al.* (2009)). We thus hypothesise that the 563-bp sequence of the *PI*^{WT} allele, substituted for 160-bp in *PI*^{POL}, contains putative regulatory sequences for establishing the correct expression pattern of the gene. By comparing *VRT2* intron-1 sequences across Poaceae, we identified two distinct motifs (both within the 563-bp region of intron 1) that showed a high degree of sequence conservation across 60 million years of evolution. The absence of the 563-bp intron-1 sequence, as in *PI*^{POL}, results in a misexpression of *VRT-A2*, both in terms of its absolute expression levels and spatiotemporal patterns. It is thus tempting to speculate that either one or both conserved intron-1 motifs allows the binding of proteins or protein complexes that repress *VRT-A2* expression. Alternatively, the *PI*^{POL} 160-bp substitution could contain sequences for positive transcriptional regulators, which could drive the higher and ectopic expression of *VRT-A2*. The B- and D-homoeologs of *VRT2* also contain the two highly conserved intron-1 motifs, and as such we see no difference in their expression pattern between NILs nor in the transgenic lines. Likewise, no changes in expression of the closest MADS-box ortholog (*TaSVPI*) were detected in *PI* NILs nor *VRT-A2* transgenic lines, similar to the lack of expression differences in closely related MADS-box genes in the maize *Tu1* mutants (Han *et al.*, 2012; Wingen *et al.*, 2012). This suggests that *VRT-A2* does not regulate its homoeologs or is unable to overcome the presence of the putative repressive protein or protein complex in intron 1 of the B- and D-genome homoeologs. Further work is needed to fully characterise the role of these putative motifs and how they regulate expression of *VRT2*.

Major loci that control a relatively large proportion of phenotypic variation for quantitative traits have been selected during domestication of diploid plant species (reviewed in Swinnen *et al.*

(2016)). Often, the causal variants underlying these phenotypes occur in *cis*-regulatory regions of developmental regulators that affect the level or the spatiotemporal expression profile of transcription factors (Sieburth and Meyerowitz, 1997; Salvi *et al.*, 2007; Louwers *et al.*, 2009; Studer *et al.*, 2011). Selection of *cis*-regulatory variation has also played a pivotal role in shaping polyploid wheat domestication. Examples include the major vernalisation (*VRN1*; (Yan *et al.*, 2003)) and photoperiod (*Ppd1*; (Wilhelm *et al.*, 2009)) response genes as well as in the major homoeolog pairing *Ph1* locus (Rey *et al.*, 2017). All these selected wheat domestication alleles are dominant or semi-dominant, thereby circumventing functional redundancy and allowing the rapid detection of favourable phenotypes.

The *PI^{POL}* allele provides a compelling example, where the over- and extended expression of *VRT-A2* results in enhancement of traits of agronomic interest in a dosage-dependent (semi-dominant) manner. This is similar to recent results in maize, where increasing and extending the expression of the MADS-box gene *ZMM28* resulted in improved vegetative and reproductive growth parameters, which impacted positively on yield (Wu *et al.*, 2019). Interestingly, the authors discuss how a more subtle over- and extended expression of *ZMM28* using a native maize promoter resulted in more consistent yield benefits and fewer pleiotropic effects compared to promoters with constitutive overexpression. Analogously, overexpression related *SVP* genes in barley (Trevaskis *et al.*, 2007) and rice (Sentoku *et al.*, 2005) using the maize Ubiquitin promoter (in both studies) resulted in multiple negative pleiotropic effects, including floral reversion. These results highlight how the more subtle changes in expression profiles, through variation in *cis*-regulation, can impact on agronomic traits. Recent work in tomato has shown how a wide range of phenotypic variation for quantitative traits can be engineered by genome editing of transcription factor promoters to generate *cis*-regulatory alleles (Rodríguez-Leal *et al.*, 2017). It will be important to determine if engineered *cis*-regulatory variants will overcome functional redundancy and have similar impact on agronomic traits in a polyploid context.

In summary, we identified *VRT2*, a member of the *SVP* family of MADS-box transcription factors, as the gene underlying the *T. polonicum* *PI* locus in polyploid wheat. An intron-1 sequence substitution results in the misexpression of *VRT-A2*, which leads to multiple phenotypic effects in a dosage dependent manner. Allelic variation studies support the intron-1 mutation in *VRT-A2* as the *T. polonicum* species defining polymorphism. The *PI^{POL}* allele increases grain weight and other agronomic traits, but not yield, in UK environments. As expression levels of *VRT-A2* are correlated with the magnitude of the phenotypic effects, it is possible that engineering of *VRT2* expression

patterns through novel *cis*-regulatory alleles will generate further beneficial quantitative variation for plant breeding.

Materials and Methods

Germplasm

To develop *PI* NILs, we crossed *T. polonicum* accession 1100002 to the hexaploid spring wheat cultivar Paragon and the resulting F_1 was backcrossed four to six times to the Paragon recurrent parent. At each generation, F_1 lines exhibiting the long-glume phenotype of *T. polonicum* were selected to continue the backcrossing process. After four (BC_4) or six (BC_6) backcrosses, BC_nF_2 plants were grown and homozygous lines for *PI* selected based on glume length. Bulk seed from the BC_4F_2 or BC_6F_2 plants were used for subsequent experiments.

Field experiments and phenotyping

The *PI* NILs were evaluated in six field experiments between 2016 to 2020. Two trials (2016 BC_4 ; 2020 BC_4 and BC_6) were sown at the John Innes Centre Experimental trials site in Bawburgh, UK (52°37'50.7"N 1°10'39.7"E) and four (2017 BC_4 ; 2018, 2019 and 2020 BC_4 and BC_6) were sown at The Morley Agricultural Foundation trials site in Morley St Botolph, UK (52°33'15.1"N 1°01'59.2"E). All experiments were sown in autumn (end September-November; except 2020 which was sown in February) as yield-scale plots (6m x 1.2m) in a randomised complete block design (RCBD) with five replications and sown by grain number for comparable plant densities aiming for 275 seeds \cdot m⁻². Developmental traits were evaluated throughout the growing period and a 10-ear sample was collected at harvest for the assessment of spike, floret and grain characteristics (marked '10ES' in Supplementary Table S1). Spike length was measured as the distance between the peduncle-rachis junction and tip of the terminal floret. Plot yield, hectolitre weight, and grain moisture were measured during harvest on board the combine (Zürn 150). Final grain yield was determined per plot after adjustment to 15% grain moisture. Grain morphometric measurements were analysed using the MARVIN grain analyser (GTA Sensorik GmbH, Neubrandenburg, Germany) using ~ 400 grains of the combined grain samples.

Spike dissection and organ measurements (NILs and transgenic lines)

We measured organ size of the PI^{WT} and PI^{POL} NILs by sampling three spikes from five field blocks per NIL grown in 2019 at Morley. The spikes were dissected by hand and all organs (glume, lemma, palea, and grain) were placed on PCR film (Cat No.: AB0580, Thermofisher) from bottom

to top of the spike. The PCR films with the organs were scanned using a standard Ricoh photocopier (settings: greyscale, 600dpi). The resulting images were analysed using the Fiji “analyse particles” function, restricting analysis to particles of 0.1-5 cm² area (Schindelin *et al.*, 2012). Fiji measures particles from top-left to bottom-right of the image, thus allowing us to match position of the organ along the spike with the Fiji measurements retrospectively. To measure organ size in the transgenic T₀ lines (grown in 1 L pots under 16 hours light at 20°C and 8 hours darkness at 15°C in a controlled environment room), we hand dissected organs from two main spikes per plant. The organs were measured and analysed as described for the NILs above.

3D scanning of spikes and morphometric grain extraction

Fifteen mature spikes from both *PI* NILs grown in 2019 at Morley were used for μ CT scanning (three spikes from five field blocks per NIL). Scanning conditions were as described in Hughes *et al.* (2019). Feature extraction from the scans was performed using previously developed MATLAB-based software (Hughes *et al.*, 2017) using the following setup parameters (SE=7, voxel size=68.8, minSize=10,000 and watershed=false). The features extracted were length (calculated using the major axis of the whole grain), width, and depth (the major and minor axis of a cross-section respectively, found by selecting the grain's midpoint), volume (a complete connected pixel count per grain), and grain counts for each spike. More than 750 grains were measured per genotype. The data were checked for false positives by first removing outliers that were identified using the 0.025 upper and lower percentiles of the data. Additionally, for added robustness, manual checks were performed.

Grain developmental timecourse

The *PI* NILs grown in 2018 and 2019 at Morley were used for the grain developmental time courses. For this, we tagged 70 ears per NIL over five replicated blocks in the field at ear emergence (spike fully emerged and peduncle just visible), as described in Brinton *et al.* (2017). Ten spikes per NIL were collected at five (2018) and six (2019) different timepoints. These were ear emergence, 3, 9, 16, and 22 days post anthesis (dpa) in 2018, while in 2019, the timepoints included ear emergence, anthesis (here measured as anther extrusion), 7, 14, 21, and 28 dpa. Grain measurements were performed as described in Brinton *et al.* (2017).

Cell size measurements

We measured cell size of mature grains from PI^{WT} and PI^{POL} NILs collected from three field blocks grown at Morley in 2019. Within each block, we sampled three spikes and from each spike we sampled grains from florets 2 and 4 of the two central spikelets. In total, this resulted in 18 grains per genotype per floret position (2 grains x 3 spikes x 3 field blocks). Dry grain samples were mounted crease-down onto 12.5 mm diameter aluminium pin stubs using double-sided 12 mm adhesive carbon discs (Agar Scientific Ltd, Stansted, Essex). The stubs were then sputter coated with approximately 15nm gold in a high-resolution sputter coater (Agar Scientific Ltd) and transferred to a Zeiss Supra 55 VP FEG scanning electron microscope (Zeiss SMT, Germany). The samples were viewed at 3kV with a magnification of 1500x and digital TIFF files were stored. The surface of each grain was imaged in the top, middle and bottom thirds of the grain (excluding the embryo; Supplementary Figure S6) with three images taken in each section (nine images total per grain). Cell length was measured manually using the Fiji distribution of ImageJ (Schindelin *et al.*, 2012). For statistical analyses, only images with ≥ 30 cell measurements were used. For each image, the median cell length was calculated. The image medians were then used to calculate a median cell length value for each section (bottom/middle/top) of each grain.

Genetic Mapping of PI

For fine-mapping, we generated a set of BC₄ and BC₆ recombinant inbred lines (RILs) derived from the PI NILs. In the first round we identified 17 BC₄F₂ heterozygous recombinant lines between markers $S1$ and $S9$. We screened twelve BC₄F₃ progeny for each line to identify homozygous recombinants, which were phenotyped for glume length (Supplementary Table S7). To further define the PI interval, we screened an additional 1867 BC₆F₂ plants heterozygous across the $S2$ and $S7$ interval. We identified 64 independent homozygous recombinants between markers $S2$ and $S10$, which were phenotyped for glume length and genotyped with a further 21 markers (Supplementary Table S8). The eight critical recombinants (Supplementary Table S9) were grown at the John Innes Centre Experimental trials site and phenotyped for height, grain weight, spike length and grain morphometrics.

To test the isogenic nature of the BC₄ PI NILs, we used the Axiom 35k Breeders' Array (Allen *et al.*, 2017). The array showed that 98.7% of markers (32839) were monomorphic between the NILs, with 418 polymorphisms between the NILs. More than 65% of the polymorphisms (272) were located on chromosome 7A, while the remaining were distributed evenly across other chromosomes. To generate markers, we performed exome-capture of an accession of *T. polonicum* (idPlant: 27422, GRU Store Code: T1100002), wildtype Paragon, and wildtype Langdon. These

three samples were exome-sequenced in a pool of eight samples on a single Illumina HiSeq2000 lane following published protocols (Krasileva *et al.*, 2017). This generated 27919048, 30795964, and 30683631 reads for the three lines, respectively. The reads were mapped to the RefSeqv1.0 (IWGSC *et al.*, 2018) assembly using bwa-0.7.15 (bwa mem -t 8 -M; (Li and Durbin, 2009; Li, 2013)). The resulting SAM file was converted to BAM format using samtools-1.3.1 (samtools view -b -h; (Li *et al.*, 2009)) and sorted by chromosome position (samtools sort). Optical and PCR duplicates were marked using picard-1.134 (picard MarkDuplicates MAX_FILE_HANDLES_FOR_READ_ENDS_MAP=1024 VALIDATION_STRINGENCY=LENIENT <http://broadinstitute.github.io/picard/>). Single nucleotide polymorphisms (SNPs) were called for chromosome 7A with freebayes-1.1.0 (freebayes -0 -t; (Garrison and Marth, 2012)), and filtered using bcftools-1.3.1 (bcftools filter; (Li and Durbin, 2009)). Lastly, the vcf file was compressed with bgzip, indexed with tabix-0.2.6 (tabix -p vcf; (Li and Durbin, 2009)) before extracting relevant data in a user-friendly format with bcftools-1.3.1 (bcftools query -H -f '%CHROM\t%POS\t%REF\t%ALT{0}\t%QUAL\t%INFO/DP\t%INFO/RO\t%INFO/AO{0}[\t%GT\t%DP\t%RO\t%AO{0}]\n'). The SNPs were filtered for polymorphisms between *T. polonicum* and the two cultivars Paragon and Langdon. These putative SNPs were used to design KASP markers using PolyMarker (Ramirez-Gonzalez *et al.*, 2015). KASP assays were validated in the parental NILs and then used for genetic mapping of *PI* as indicated in Supplementary Tables S7-S8.

PCR markers

The mapping populations were genotyped as described in Trick *et al.* (2012), with the following changes: 2 µl DNA (10-40 ng) was mixed with 2 µl of mastermix (2 µl PACE (Standard ROX; 3CR Bioscience) with 0.056 µl primer assay) for a total reaction volume of 4 µl. All PACE markers used for map-based cloning are listed in Supplementary Table S18. Standard PCR as well as qRT-PCR primers, their annealing temperatures and amplicon sizes are listed Supplementary Table S19.

TraesCS7A02G175200 gene model

Using the expVIP browser (Borrill *et al.*, 2016; Ramírez-González *et al.*, 2018), expression of *TraesCS7A02G175200* showed high expression in young seedlings (vegetative plants with 1 cm long spikes). The corresponding transcriptome data (Zadoks growth stage 30; (Choulet *et al.*, 2014)) was downloaded, and aligned to the genomic RefSeqv1.0 assembly using HiSat2 v2.1.0 (hisat2 -p 16; (Kim *et al.*, 2015)). The SAM file was converted to BAM format, sorted, and optical duplicates

were marked as described for the exome capture data above. The depth of reads was measured using samtools-1.3.1 (samtools depth -a). The RNA-seq data supports the *TraesCS7A02G175200.1* gene model and its predicted untranslated regions (UTRs; Supplementary Figure S7B).

Phylogenetic analysis of StMADS11-like family

Amino acid sequences of StMADS11 and related proteins were aligned using MUSCLE with default settings using the EBI web services (Edgar, 2004a, b; Madeira *et al.*, 2019). The resulting phylogenetic tree was visualized in FigTree v1.4.3 (<http://tree.bio.ed.ac.uk/software/figtree/>). A list of all proteins used for the alignment can be found in Supplementary Table S20.

Haplotype variation of *TraesCS7A02G175200*

We sequenced the promoter (2299 bp), *TraesCS7A02G175200* genomic sequence (5591 bp, exon and introns) and 1857 bp downstream of the termination codon (9747 bp) in the *PI^{POL}* NIL using primers detailed in Supplementary Table S19. We also sequenced the 5591 bp exon-intron sequences of *TraesCS7A02G175200* in six *T. polonicum*, two *T. petropavlovskyi*, and four ‘Arrancada’ accessions (Supplementary Table S12) using primers listed in Supplementary Table S19.

We developed a PCR marker (primers S37_Fwd and S37_Rev; Supplementary Table S19) to determine the presence of either the 563-bp or the 160-bp intron-1 substitution in a large diversity panel. We used this marker to assay the intron-1 status of 70 wild emmer (*T. dicoccoides*), 103 hexaploid landraces, 4 durum, 23 *T. polonicum*, 2 *T. petropavlovskyi* and 7 ‘Arrancada’ landrace accessions. We also used available genome sequences of 16 hexaploid (Walkowiak *et al.*, in press) and 3 tetraploid (Avni *et al.*, 2017; Maccaferri *et al.*, 2019; Walkowiak *et al.*, in press) cultivars and accessions to characterise *TraesCS7A02G175200* across its promoter, exon-intron sequences and 3’ untranslated region (Supplementary Table S10). We also evaluated the wider haplotype of the *PI* NILs, 16 hexaploid and 1 tetraploid cultivar, 7 *T. polonicum*, 2 *T. petropavlovskyi* and 7 ‘Arrancada’ landrace accessions using 14 markers spanning the 7A physical region (Supplementary Table S13). Details of the accessions used are listed in Supplementary Tables S11 and S12.

Phylogenetic footprinting

We extracted intron 1 sequences of *VRT2* orthologs from barley (Horvu7Hr1G036130), *Brachypodium* (Bradi1g45812), rice (Os06g0217300), maize (GRMZM5G814279) and sorghum

(SORBI_3010G085400) and used these, alongside *TraesCS7A02G175200*, as query sequences in the mVISTA program (<http://genome.lbl.gov/vista/index.shtml>).

Intron-1 motif discovery

The phylogenetic footprinting analysis revealed two conserved sequence peaks between wheat, barley, *Brachypodium*, rice, maize, and sorghum. These sequences, plus some flanking sequence (71 and 84 bp for both regions, respectively), were aligned using T-coffee with default settings (<https://www.ebi.ac.uk/Tools/msa/tcoffee/>; (Notredame *et al.*, 2000; Madeira *et al.*, 2019)). We defined the motifs using the following approach: a nucleotide was considered conserved if it was identical in 5 out of the 6 species (83%). A maximum of four nucleotides with lower conservation was tolerated, provided the neighbouring sequences were again highly conserved (83%). This yielded a 34 and 69 bp sequence, which were designated Motif 1 and Motif 2, respectively (Supplementary Data Set S1). When tolerating only a single nucleotide with low conservation (<83%), a highly conserved 16 and 20 bp sequence was detected within Motif 1 and Motif 2, respectively (Supplementary Data Set S1). In addition, within Motif 2, we detected a 6 bp highly conserved palindromic sequence that we designated “palindrome” (Supplementary Data Set S1).

Transcription factor binding site analysis of predicted motifs

To search for possible transcription factor binding sites within the predicted motif sequences we used three different tools. The sequences were queried one by one using the Binding Site Prediction tool from PlantRegMap (http://plantregmap.gao-lab.org/binding_site_prediction.php) with default settings for the *Arabidopsis thaliana*, *Oryza sativa*, and *Zea mays* databases respectively (Tian *et al.*, 2020). Next, we queried the *Arabidopsis thaliana*, *Oryza sativa*, and *Zea mays* databases of PlantPan3.0 using the TF/TFBS Search tool with a q-value cut-off of 0.05. Lastly, we used the Tomtom tool of MEME Suite 5.2.0 (<http://meme-suite.org/tools/tomtom>) to query the *Arabidopsis thaliana* DAP motifs database from O'Malley *et al.* (2016) as well as the ‘JASPAR CORE (2018) plants’ database (Khan *et al.*, 2018) with default settings.

RNA extraction

BC₄ NILs were grown in 11 cm² pots (1 L volume) in ‘John Innes Cereal Mix’ (40% Medium Grade Peat, 40% Sterilised Soil, 20% Horticultural Grit, 1.3 kg*m⁻³ PG Mix 14-16-18 + Te Base Fertiliser, 1 kg*m⁻³ Osmocote Mini 16-8-11 2 mg + Te 0.02% B, Wetting Agent, 3 kg*m⁻³ Maglime, 300 g*m⁻³ Exemptor) under long day conditions (16 h light : 8 h dark) in the glasshouse.

Tissues were harvested, immediately placed into 2 ml tubes in liquid nitrogen and stored at -80°C until needed. For meristem tissues, samples were dissected using a stereo microscope (Leica MZ16) and processed as above. Details of tissues sampled are presented in Supplementary Table S14. For transgenic plants, we sampled flag leaves, glumes, and grains at 21 days post anthesis.

The grain samples were homogenized using mortar and pestle with liquid nitrogen. All other tissues were homogenized in a SPEX CertiPrep 2010-230 Geno/Grinder (Cat No.: 12605297, Fischer Scientific) using 5 mm steel beads (Cat No.: 69989, Qiagen); tubes were shaken in 20 sec bursts at 1500 rpm, then immediately transferred back into liquid nitrogen. Depending on the tissue type, this was repeated up to two times.

RNA was extracted using three different methods depending on the tissue:

- (a) For young spikes (up until Floret primordium stage W3.5), we used the Qiagen RNeasy Plant Mini Kit (Cat No.: 74904, Qiagen) with RLT buffer according to the manufacturer's protocol, as it enables recovery of RNA from small input samples. DNA digestion was performed using the RNase-Free DNase Set (Cat No.: 79254, Qiagen) according to the manufacturer's protocol.
- (b) For all other non-grain tissues, we used the Spectrum Plant Total RNA kit (Cat No.: STRN250-1KT, Sigma), following Protocol A of the manufacturer's protocol and using 750 µL of Binding Solution. DNA digestion was performed using the On-Column DNase I Digestion Set (Cat No.: DNASE70-1SET, Sigma) according to the manufacturer's protocol.
- (c) For grain samples, 500 µL of RNA extraction buffer (0.1 M Tris pH 8.0, 5 mM EDTA pH 8.0, 0.1 M NaCl, 0.5% SDS; autoclaved) with 1% β-Mercaptoethanol (Cat No.: M3148, Merck) and 100 µL of Ambion Plant RNA Isolation Aid (Cat No.: AM9690, Thermofisher) were added to each sample, before vortexing. Tissue debris as well as polysaccharides and polyphenols were pelleted at 13000 rpm for 10 min in a microcentrifuge. The supernatant was transferred to a new 1.5 mL tube, before adding 500 µL of Acid Phenol:Chloroform:IAA (125:24:1) (Cat No.: AM9720, Thermofisher). The tubes were shaken in a SPEX CertiPrep 2010-230 Geno/Grinder for 10 min at 500 rpm, then placed in a microcentrifuge at 13000 rpm for 15 min to separate the organic and aqueous components. The supernatant (aqueous phase) was transferred to a new 1.5 mL tube with 500 µL of Chloroform (Cat No.: C/4960/PB17, FisherScientific). The tubes were inverted 10 times and then placed in a microcentrifuge for 15 min at 13000 rpm. The supernatant was transferred to a new 1.5 mL tube with 360 µL of Isopropanol (Cat No.: P/7500/PC17, FisherScientific) and 45 µL 3 M Sodium Acetate (pH 5.2). The tube was inverted 10 times to mix the solution, before placing at 4°C for 1 hour to precipitate RNA. The RNA was pelleted in a

microcentrifuge at 4°C by spinning for 30 min at 13000 rpm. The supernatant was carefully tipped off to not lose the pellet. The tubes were then washed twice with 70% Ethanol (Cat No.: 20821.330, VWR) and centrifuged between washes at 13000 rpm for 5 min at 4°C. The supernatant was then carefully discarded and remaining droplets of Ethanol removed using a pipette tip, before adding 100 µL of nuclease-free water (Cat No.: AM9937, Thermofisher).

Quantitative real-time reverse-transcription PCR (qRT-PCR)

RNA was reverse transcribed using M-MLV reverse transcriptase (Cat No.: 28025013, Thermofisher) according to the manufacturer's protocol. For the qRT-PCR reactions, LightCycler 480 SYBR Green I Master Mix (Roche Applied Science, UK) was used according to the manufacturer's protocol. The reactions were run in a LightCycler 480 instrument (Roche Applied Science, UK) under the following conditions: 5 min at 95 °C; 45 cycles of 10 s at 95 °C, 15 s at 62 °C, 30 s at 72 °C; dissociation curve from 60 °C to 95 °C to determine primer specificity. All reactions were performed with three technical replicates per sample and using *TaActin* as reference gene (Li *et al.*, 2019). Relative gene expression was calculated using the $2^{-\Delta\Delta C_t}$ method (Livak and Schmittgen, 2001) with a common calibrator so that values are comparable across genes, tissues and developmental stages. All primers used in qRT-PCR are listed in Supplementary Table S19.

Construct assembly

A modified version of the GoldenGate (MoClo) compatible level 2 vector pGoldenGreenGate-M (pGGG-M) as described in Hayta *et al.* (2019) was used in this study. The pGGG-AH-L2P2 acceptor plasmid is comprised of the hygromycin resistance gene (hpt) containing the Cat1 intron driven by the rice actin1 (*OsAct1*) promoter for *in planta* selection and a LacZ-MCS flanked by two *BsaI* sites at MoClo position 2 with standardised overhangs to accept basic (level 0) components. In brief, the *T. polonicum* VRT-A2 promoter (2299 bp), genomic sequence (5585 bp), 1000 bp downstream of STOP codon, and NOS terminator (8916 bp total) were cloned into pGGG-AH-L2P2 using standard Golden Gate MoClo assembly (Werner *et al.*, 2012), resulting in construct pGGG-AH-VRT-A2 (Supplementary Figure S9). Several *BsaI* and *BbsI* sites had to be domesticated to make the *T. polonicum* VRT-A2 sequence suitable for Golden Gate MoClo assembly, including 3 sites in the promoter (C494T, G869A, C2075T), 1 site in exon 1 (C2440T; V47V), 1 site in an intronic MITE (C4691T), and 1 site in exon 3 (T5791C; L106L). Six nucleotides from a partial LINE in intron 5 were omitted by mistake from the genomic sequence. The construct was electroporated into the hypervirulent *Agrobacterium tumefaciens* strain AGL1 (Lazo *et al.*, 1991) containing the helper

plasmid pAL155 (additional *VirG* gene). Standard inoculums of *Agrobacterium* (Tingay *et al.*, 1997) were prepared as described in Hayta *et al.* (2019).

Wheat transformation

Hexaploid wheat c.v. ‘Fielder’ was transformed using the previously described method by Hayta *et al.* (2019). In brief, under aseptic conditions wheat immature embryos were isolated, pre-treated by centrifugation, inoculated with *A. tumefaciens* AGL1 containing pGGG-AH-VRT-A2 and co-cultivated for 3 days. Wheat callus proliferation, shoot regeneration, and rooting were carried out under a stringent hygromycin selection regime before the regenerated plantlets were transferred from *in vitro* to soil and acclimatised. Transgenesis was confirmed by *hpt* gene PCR; transgene copy number analysis was performed using Taqman qPCR and probe (Hayta *et al.*, 2019). The values obtained were used to calculate copy number according to published methods (Livak and Schmittgen, 2001). Based on this copy number determination we defined T₀ lines as zero, low (1 to 2 copies of pGGG-AH-VRT-A2), medium (4-5 copies of pGGG-AH-VRT-A2) and high (9 or more copies of pGGG-AH-VRT-A2) copy number lines (Supplementary Table S15).

Statistical Analyses

Field experiments: To determine the differences between the PI^{POL} and PI^{WT} NILs, we performed ANOVA on the multiple field phenotypic data in RStudio (v1.3.1056). For the overall analysis we included block (nested in location), genotype, location, and the genotype*location interaction in the model. For the analysis of individual locations, we used a simple two-way ANOVA including block and genotype. For the BC₆ RILs, we determined the effect of the *VRT-A2* allele on height, TGW, spike length, grain width and length using a two-way ANOVA using block and the *VRT-A2* genotype in the model. For glume length, RILs were assigned as having a normal or long-glume phenotype using a *post hoc* Dunnett's test to compare with the PI^{POL} and PI^{WT} controls.

Spike dissection: We used glume measurements from spikelets 1 to 20 to determine the differences between the PI^{POL} and PI^{WT} NILs. Given that the experimental unit is the field plot to which the genotype was randomised within each block, we analysed the data using a split-plot ANOVA in which the ‘Spikelet’ was nested within the ‘Genotype*Block’ interaction. The ANOVA therefore included the following terms: Block, Genotype, Spikelet and Genotype*Spikelet interactions, with *F* statistic and *P* values calculated based on the ‘Block*Genotype’ error term (for Block and Genotype) or the Residual error term for the other factors.

We analysed the grain, lemma, and palea data from spikelets 1 to 20 and florets 1 to 4 to determine the differences between the *PI* NILs. Given that the florets are nested in the spikelet, and the spikelet is nested within the genotype*block interaction (i.e. the florets and spikelets are not randomly assigned), we analysed the data as a split-split plot design using the corresponding error terms for calculating the *F* statistic and *P* values. This model included the block, genotype, spikelet, floret, and corresponding interaction terms. We also performed individual ANOVAs for each floret position using the same model as above, with the exception that we excluded floret as a factor.

Grain development timecourse: Each block at every timepoint consisted of c. 100 grains (10 spikes x 10 grains) per NIL. The grain morphometrics were averaged across the 100 grains (as they were considered to be subsamples) to yield a single value per timepoint, resulting in 5 datapoints per NIL per timepoint. We performed a two-way ANOVA with Block and Genotype in the model to determine whether *PI* affects grain morphometrics at the sampled timepoints.

Cell size measurements: We analysed the data independently for floret 2 and 4 using a three-way ANOVA including Block, Genotype, Block*Genotype, Section, and the Genotype*Section interaction. Given the significant Genotype*Section interactions, we explored differences between *PI* genotypes for each section using Tukey multiple comparison as implemented in RStudio (v1.3.1056).

Expression: We evaluated differences in expression levels of *VRT2* and *MADS22* homoeologs by performing t-tests between the $2^{-\Delta\Delta Ct}$ expression values of *PI^{POL}* and *PI^{WT}* NILs for each individual tissue*timepoint comparison.

Phenotypes in transgenic lines: To evaluate differences in phenotype between the four categories of transgenic lines (zero, low, medium, and high copy number lines; Supplementary Table S16) we performed one-way ANOVAs for each floret position including ‘transgene copy number’ as the single factor. Given that ‘transgene copy number’ was significant for all phenotypes (glume, lemma, palea, and grain length) and across all florets, we performed Tukey multiple comparison tests to determine differences between the four ‘transgene copy number’ categories as well as Dunnett tests against the zero copy number control lines (Supplementary Table S16).

Correlation of phenotype and expression in transgenic T0 lines: We calculated the Pearson’s correlation coefficient between *VRT-A2* expression (in flag leaf, glume, and grain) and phenotypic traits (internode length, spike length, glume length, lemma length, grain length, palea length) in R (Supplementary Table S17). We used `geom_smooth(method = “lm”)` to plot the regression line and 95% confidence interval.

Acknowledgements

This work was supported by the UK Biotechnology and Biological Sciences Research Council (BBSRC) through the grant BB/S016945/1, BB/S016538/1, the Designing Future Wheat (BB/P016855/1), the National Capability in Plant Phenotyping (BBS/E/W/0012844A) and Genes in the Environment (BB/P013511/1) Institute Strategic Programmes. We thank the JIC Field Trials and Horticultural Services teams for technical support in field and glasshouse experiments and Karen Askew for uCT support.

Author Contributions

JS, NMA, and CU conceived the study. JS generated the NILs and mapping populations together with PS. NMA performed most experiments. AP and OH genotyped Watkins, *T. dicoccoides*, and *T. polonicum* accessions using a PCR marker and sequenced amplicons. YC analysed VRT-A2 alleles in publicly available genome data. AEB dissected spikelets of NILs, phenotyped and assessed the data. The grains of these lines were imaged by JFB and EB using scanning electron microscopy, with JFB analysing the data. MS designed and created the pGGG-AH-VRT-A2 construct; SH transformed cv. Fielder with the construct, cultivated the plants and performed copy number analysis on them. JS performed field experiments and phenotyping. TF and PC helped with plant husbandry, phenotyping, and data collection. MC, JD, and CN performed CT-scans of field-grown spikelets and analysed the data. CU performed statistical analysis of all data. JFB created the figures. NMA and CU wrote the manuscript. All authors have read and approved the manuscript.

References

- Akond, A.S.M.G., and Watanabe, N.** (2005). Genetic variation among portuguese landraces of 'Arrancada' wheat and *Triticum petropavlovskyi* by AFLP-based assessment. *Genet Resour Crop Ev* **52**, 619-628.
- Akond, A.S.M.G.M., Watanabe, N., and Furuta, Y.** (2008). Comparative genetic diversity of *Triticum aestivum* - *Triticum polonicum* introgression lines with long glume and *Triticum petropavlovskyi* by AFLP-based assessment. *Genet Resour Crop Ev* **55**, 133-141.
- Allen, A.M., Winfield, M.O., Burrige, A.J., Downie, R.C., Benbow, H.R., Barker, G.L.A., Wilkinson, P.A., Coghill, J., Waterfall, C., Davassi, A., et al.** (2017). Characterization of a Wheat Breeders' Array suitable for high-throughput SNP genotyping of global accessions of hexaploid bread wheat (*Triticum aestivum*). *Plant Biotechnology Journal* **15**, 390-401.
- Avni, R., Nave, M., Barad, O., Baruch, K., Twardziok, S.O., Gundlach, H., Hale, I., Mascher, M., Spannagl, M., Wiebe, K., et al.** (2017). Wild emmer genome architecture and diversity elucidate wheat evolution and domestication. *Science* **357**, 93.

- Biffen, R.H.** (1905). Mendel's laws of inheritance and wheat breeding. *The Journal of Agricultural Science* **1**, 4-48.
- Borrill, P., Ramirez-Gonzalez, R., and Uauy, C.** (2016). expVIP: a customizable RNA-seq data analysis and visualization platform. *Plant Physiology* **170**, 2172.
- Brinton, J., Simmonds, J., Minter, F., Leverington-Waite, M., Snape, J., and Uauy, C.** (2017). Increased pericarp cell length underlies a major quantitative trait locus for grain weight in hexaploid wheat. *New Phytologist* **215**, 1026-1038.
- Charles, M., Tang, H., Belcram, H., Paterson, A., Gornicki, P., and Chalhouh, B.** (2009). Sixty million years in evolution of soft grain trait in grasses: emergence of the softness locus in the common ancestor of Pooideae and Ehrhartoideae, after their divergence from Panicoideae. *Molecular Biology and Evolution* **26**, 1651-1661.
- Chen, P.D., D.J., L., G.Z., P., L.L., Q., and L., H.** (1988). The chromosome constitution of three endemic hexaploid wheats in Western China. In 7th Int. Wheat Genet. Symp, M. T.E. and K. R.M.D., eds (Cambridge, UK), pp. 75-80.
- Chen, Q., Y., S., and Y., D.** (1985). Cytogenetic studies on interspecific hybrids of Xinjiang wheat. *Acta Agron Sin* **11**, 23-28.
- Choulet, F., Alberti, A., Theil, S., Glover, N., Barbe, V., Daron, J., Pingault, L., Sourdille, P., Couloux, A., Paux, E., et al.** (2014). Structural and functional partitioning of bread wheat chromosome 3B. *Science* **345**, 1249721.
- Distelfeld, A., Li, C., and Dubcovsky, J.** (2009). Regulation of flowering in temperate cereals. *Current Opinion in Plant Biology* **12**, 178-184.
- Edgar, R.C.** (2004a). MUSCLE: a multiple sequence alignment method with reduced time and space complexity. *BMC Bioinformatics* **5**, 113.
- Edgar, R.C.** (2004b). MUSCLE: multiple sequence alignment with high accuracy and high throughput. *Nucleic Acids Research* **32**, 1792-1797.
- Engledow, F.L.** (1920). The inheritance of glume-length and grain-length in a wheat cross. *Journal of Genetics* **10**, 109-134.
- Frazer, K.A., Pachter, L., Poliakov, A., Rubin, E.M., and Dubchak, I.** (2004). VISTA: computational tools for comparative genomics. *Nucleic Acids Research* **32**, W273-W279.
- Garrison, E., and Marth, G.** (2012). Haplotype-based variant detection from short-read sequencing. *arXiv* **1207.3907**.
- Gregis, V., Andrés, F., Sessa, A., Guerra, R.F., Simonini, S., Mateos, J.L., Torti, S., Zambelli, F., Prazzoli, G.M., Bjerkan, K.N., et al.** (2013). Identification of pathways directly regulated by SHORT VEGETATIVE PHASE during vegetative and reproductive development in *Arabidopsis*. *Genome Biology* **14**, R56.
- Han, J.-J., Jackson, D., and Martienssen, R.** (2012). Pod corn is caused by rearrangement at the *Tunicate1* locus. *The Plant Cell* **24**, 2733.
- Hayta, S., Smedley, M.A., Demir, S.U., Blundell, R., Hinchliffe, A., Atkinson, N., and Harwood, W.A.** (2019). An efficient and reproducible *Agrobacterium*-mediated transformation method for hexaploid wheat (*Triticum aestivum* L.). *Plant Methods* **15**, 121.
- Hughes, N., Oliveira, H.R., Fradgley, N., Corke, F.M.K., Cockram, J., Doonan, J.H., and Nibau, C.** (2019). μ CT trait analysis reveals morphometric differences between domesticated temperate small grain cereals and their wild relatives. *The Plant Journal* **99**, 98-111.
- Hughes, N., Askew, K., Scotson, C.P., Williams, K., Sauze, C., Corke, F., Doonan, J.H., and Nibau, C.** (2017). Non-destructive, high-content analysis of wheat grain traits using X-ray micro computed tomography. *Plant Methods* **13**, 76.
- IWGSC, T.I.W.G.S.C., Appels, R., Eversole, K., Stein, N., Feuillet, C., Keller, B., Rogers, J., Pozniak, C.J., Choulet, F., Distelfeld, A., et al.** (2018). Shifting the limits in wheat research and breeding using a fully annotated reference genome. *Science* **361**, eaar7191.
- Kane, N.A., Agharbaoui, Z., Diallo, A.O., Adam, H., Tominaga, Y., Ouellet, F., and Sarhan, F.** (2007). TaVRT2 represses transcription of the wheat vernalization gene *TaVRN1*. *The Plant Journal* **51**, 670-680.
- Kane, N.A., Danyluk, J., Tardif, G., Ouellet, F., Laliberté, J.-F., Limin, A.E., Fowler, D.B., and Sarhan, F.** (2005). *TaVRT-2*, a member of the StMADS-11 clade of flowering repressors, is regulated by vernalization and photoperiod in wheat. *Plant physiology* **138**, 2354-2363.

- Khan, A., Fornes, O., Stigliani, A., Gheorghe, M., Castro-Mondragon, J.A., van der Lee, R., Bessy, A., Chèneby, J., Kulkarni, S.R., Tan, G., *et al.* (2018). JASPAR 2018: update of the open-access database of transcription factor binding profiles and its web framework. *Nucleic Acids Research* **46**, D260-D266.
- Kim, D., Langmead, B., and Salzberg, S.L. (2015). HISAT: a fast spliced aligner with low memory requirements. *Nature Methods* **12**, 357-360.
- Kosuge, K., Watanabe, N., and Kuboyama, T. (2010). Recombination around the *P* locus for long glume phenotype in experimental introgression lines of *Triticum aestivum* – *Triticum polonicum*. *Genet Resour Crop Ev* **57**, 611-618.
- Krasileva, K.V., Vasquez-Gross, H.A., Howell, T., Bailey, P., Paraiso, F., Clissold, L., Simmonds, J., Ramirez-Gonzalez, R.H., Wang, X., Borrill, P., *et al.* (2017). Uncovering hidden variation in polyploid wheat. *Proceedings of the National Academy of Sciences* **114**, E913.
- Lazo, G.R., Stein, P.A., and Ludwig, R.A. (1991). A DNA transformation-competent *Arabidopsis* genomic library in *Agrobacterium*. *Bio/Technology* **9**, 963-967.
- Li, C., Lin, H., Chen, A., Lau, M., Jernstedt, J., and Dubcovsky, J. (2019). Wheat *VRN1*, *FUL2* and *FUL3* play critical and redundant roles in spikelet development and spike determinacy. *Development* **146**, dev175398.
- Li, H. (2013). Aligning sequence reads, clone sequences and assembly contigs with BWA-MEM. *arXiv* **1303.3997**.
- Li, H., and Durbin, R. (2009). Fast and accurate short read alignment with Burrows–Wheeler transform. *Bioinformatics* **25**, 1754-1760.
- Li, H., Handsaker, B., Wysoker, A., Fennell, T., Ruan, J., Homer, N., Marth, G., Abecasis, G., Durbin, R., and Genome Project Data Processing, S. (2009). The Sequence Alignment/Map format and SAMtools. *Bioinformatics* **25**, 2078-2079.
- Livak, K.J., and Schmittgen, T.D. (2001). Analysis of relative gene expression data using real-time quantitative PCR and the $2^{-\Delta\Delta CT}$ method. *Methods* **25**, 402-408.
- Louwers, M., Bader, R., Haring, M., van Driel, R., de Laat, W., and Stam, M. (2009). Tissue- and expression level-specific chromatin looping at maize *b1* epialleles. *The Plant Cell* **21**, 832.
- Maccaferri, M., Harris, N.S., Twardziok, S.O., Pasam, R.K., Gundlach, H., Spannagl, M., Ormanbekova, D., Lux, T., Prade, V.M., Milner, S.G., *et al.* (2019). Durum wheat genome highlights past domestication signatures and future improvement targets. *Nature Genetics* **51**, 885-895.
- Madeira, F., Madhusoodanan, N., Lee, J., Tivey, A.R.N., and Lopez, R. (2019). Using EMBL-EBI Services via Web Interface and Programmatically via Web Services. *Current Protocols in Bioinformatics* **66**, e74.
- Matsumura, S. (1950). Linkage study in wheat. II. *P*-linkage group and the manifold effects of the *P* gene. *Jpn J Genet* **25**, 111-118.
- Mayor, C., Brudno, M., Schwartz, J.R., Poliakov, A., Rubin, E.M., Frazer, K.A., Pachter, L.S., and Dubchak, I. (2000). VISTA : visualizing global DNA sequence alignments of arbitrary length. *Bioinformatics* **16**, 1046-1047.
- Millet, E. (1986). Relationships between grain weight and the size of floret cavity in the wheat spike. *Annals of Botany* **58**, 417-423.
- Notredame, C., Higgins, D.G., and Heringa, J. (2000). T-coffee: a novel method for fast and accurate multiple sequence alignment. *Journal of Molecular Biology* **302**, 205-217.
- O'Malley, R.C., Huang, S.-S.C., Song, L., Lewsey, M.G., Bartlett, A., Nery, J.R., Galli, M., Gallavotti, A., and Ecker, J.R. (2016). Cistrome and Epicistrome Features Shape the Regulatory DNA Landscape. *Cell* **165**, 1280-1292.
- Okamoto, Y., and Takumi, S. (2013). Pleiotropic effects of the elongated glume gene *P1* on grain and spikelet shape-related traits in tetraploid wheat. *Euphytica* **194**, 207-218.
- Percival, J. (1921). *The wheat plant: a monograph*. (London: Duckworth and Co.).
- Ramirez-Gonzalez, R.H., Uauy, C., and Caccamo, M. (2015). PolyMarker: a fast polyploid primer design pipeline. *Bioinformatics* **31**, 2038-2039.
- Ramírez-González, R.H., Borrill, P., Lang, D., Harrington, S.A., Brinton, J., Venturini, L., Davey, M., Jacobs, J., van Ex, F., Pasha, A., *et al.* (2018). The transcriptional landscape of polyploid wheat. *Science* **361**, eaar6089.

- Reineke, A.R., Bornberg-Bauer, E., and Gu, J.** (2011). Evolutionary divergence and limits of conserved non-coding sequence detection in plant genomes. *Nucleic acids research* **39**, 6029-6043.
- Rey, M.-D., Martín, A.C., Higgins, J., Swarbreck, D., Uauy, C., Shaw, P., and Moore, G.** (2017). Exploiting the *ZIP4* homologue within the wheat *Ph1* locus has identified two lines exhibiting homoeologous crossover in wheat-wild relative hybrids. *Molecular Breeding* **37**, 95.
- Rodríguez-Leal, D., Lemmon, Z.H., Man, J., Bartlett, M.E., and Lippman, Z.B.** (2017). Engineering quantitative trait variation for crop improvement by genome editing. *Cell* **171**, 470-480.e478.
- Salvi, S., Sponza, G., Morgante, M., Tomes, D., Niu, X., Fengler, K.A., Meeley, R., Ananiev, E.V., Svitashchev, S., Bruggemann, E., et al.** (2007). Conserved noncoding genomic sequences associated with a flowering-time quantitative trait locus in maize. *Proceedings of the National Academy of Sciences* **104**, 11376.
- Schindelin, J., Arganda-Carreras, I., Frise, E., Kaynig, V., Longair, M., Pietzsch, T., Preibisch, S., Rueden, C., Saalfeld, S., Schmid, B., et al.** (2012). Fiji: an open-source platform for biological-image analysis. *Nature Methods* **9**, 676-682.
- Sentoku, N., Kato, H., Kitano, H., and Imai, R.** (2005). *OsMADS22*, an *STMADS11*-like MADS-box gene of rice, is expressed in non-vegetative tissues and its ectopic expression induces spikelet meristem indeterminacy. *Molecular Genetics and Genomics* **273**, 1-9.
- Sieburth, L.E., and Meyerowitz, E.M.** (1997). Molecular dissection of the AGAMOUS control region shows that *cis* elements for spatial regulation are located intragenically. *The Plant Cell* **9**, 355.
- Studer, A., Zhao, Q., Ross-Ibarra, J., and Doebley, J.** (2011). Identification of a functional transposon insertion in the maize domestication gene *tb1*. *Nature Genetics* **43**, 1160-1163.
- Sung, S., He, Y., Eshoo, T.W., Tamada, Y., Johnson, L., Nakahigashi, K., Goto, K., Jacobsen, S.E., and Amasino, R.M.** (2006). Epigenetic maintenance of the vernalized state in *Arabidopsis thaliana* requires LIKE HETEROCHROMATIN PROTEIN 1. *Nature Genetics* **38**, 706-710.
- Swinnen, G., Goossens, A., and Pauwels, L.** (2016). Lessons from domestication: targeting *cis*-regulatory elements for crop improvement. *Trends in Plant Science* **21**, 506-515.
- Tian, F., Yang, D.-C., Meng, Y.-Q., Jin, J., and Gao, G.** (2020). PlantRegMap: charting functional regulatory maps in plants. *Nucleic Acids Research* **48**, D1104-D1113.
- Tingay, S., McElroy, D., Kalla, R., Fieg, S., Wang, M., Thornton, S., and Brettell, R.** (1997). *Agrobacterium tumefaciens*-mediated barley transformation. *The Plant Journal* **11**, 1369-1376.
- Trevaskis, B., Tadege, M., Hemming, M.N., Peacock, W.J., Dennis, E.S., and Sheldon, C.** (2007). *Short vegetative phase*-like MADS-box genes inhibit floral meristem identity in barley. *Plant physiology* **143**, 225-235.
- Trick, M., Adamski, N.M., Mugford, S.G., Jiang, C.-C., Febrer, M., and Uauy, C.** (2012). Combining SNP discovery from next-generation sequencing data with bulked segregant analysis (BSA) to fine-map genes in polyploid wheat. *BMC Plant Biol* **12**, 14-14.
- Waddington, S.R., Cartwright, P.M., and Wall, P.C.** (1983). A quantitative scale of spike initial and pistil development in barley and wheat. *Annals of Botany* **51**, 119-130.
- Walkowiak, S., Gao, L., Monata, C., Haberer, G., Kassa, M., Brinton, J., Ramirez-Gonzalez, R., Kolodziej, M., Delorean, E., Thambugala, D., et al.** (in press). Spotlight on global wheat genome variation and impact for modern breeding.
- Watanabe, N., and Imamura, I.** (2002). Genetic control of long glume phenotype in tetraploid wheat derived from *Triticum petropavlovskyi* Udacz. et Migusch. *Euphytica* **128**, 211-217.
- Watanabe, N., Yotani, Y., and Furuta, Y.** (1996). The inheritance and chromosomal location of a gene for long glume in durum wheat. *Euphytica* **91**, 235-239.
- Watanabe, N., Bannikova, S.V., and Goncharov, N.P.** (2004). Inheritance and chromosomal location of the gene for long glume phenotype found in Portuguese landraces of hexaploid wheat, "Arrancada". *J. Genet. & Breed.* **58**, 273-278.
- Werner, S., Engler, C., Weber, E., Gruetzner, R., and Marillonnet, S.** (2012). Fast track assembly of multigene constructs using Golden Gate cloning and the MoClo system. *Bioengineered* **3**, 38-43.
- Wilhelm, E.P., Turner, A.S., and Laurie, D.A.** (2009). Photoperiod insensitive *Ppd-A1a* mutations in tetraploid wheat (*Triticum durum* Desf.). *Theoretical and Applied Genetics* **118**, 285-294.

- Wingen, L.U., Münster, T., Faigl, W., Deleu, W., Sommer, H., Saedler, H., and Theißen, G. (2012).** Molecular genetic basis of pod corn (*Tunicate* maize). *Proceedings of the National Academy of Sciences* **109**, 7115.
- Wu, J., Lawit, S.J., Weers, B., Sun, J., Mongar, N., Van Hemert, J., Melo, R., Meng, X., Rupe, M., Clapp, J., *et al.* (2019).** Overexpression of *ZMM28* increases maize grain yield in the field. *Proceedings of the National Academy of Sciences* **116**, 23850.
- Yan, L., Loukoianov, A., Tranquilli, G., Helguera, M., Fahima, T., and Dubcovsky, J. (2003).** Positional cloning of the wheat vernalization gene *VRN1*. *Proceedings of the National Academy of Sciences* **100**, 6263.